



A Review: TiO₂ based photoelectrocatalytic chemical oxygen demand sensors and their usage in industrial applications



Bersu Bastug Azer^{a,b,*}, Ahmet Gulsaran^{a,b}, Joel R. Pennings^{a,b}, Resul Saritas^{b,c}, Samed Kocer^{b,c}, Jessica L. Bennett^d, **Yash Devdas Abhang^e**, Michael A. Pope^{b,f}, Eihab Abdel-Rahman^{b,c}, Mustafa Yavuz^{a,b}

^a Department of Mechanical and Mechatronics Engineering, University of Waterloo, 200 University Ave. West, Waterloo, ON N2L 3G1, Canada

^b Waterloo Institute for Nanotechnology (WIN), University of Waterloo, 200 University Ave. West, Waterloo, ON N2L 3G1, Canada

^c Department of Systems Design Engineering, University of Waterloo, 200 University Ave. West, Waterloo, ON N2L 3G1, Canada

^d Department of Civil and Resource Engineering, Dalhousie University, 1360 Barrington St., Halifax, NS, B3H 4R2, Canada

^e MANTECH, 5473 Highway 6 North, Guelph, ON N1H 6J2, Canada

^f Department of Chemical Engineering, University of Waterloo, 200 University Ave. West, Waterloo, ON N2L 3G1, Canada

ARTICLE INFO

Keywords:

TiO₂
Photoelectrocatalysis
PeCOD
Water quality sensing
PeCOD sensing housing design and fabrication
Chemical oxygen demand

ABSTRACT

The increase in global population, industrialization and need for water security has fostered a demand for novel technologies related to water treatment and purification. The oxygen demand of a given water matrix can provide useful information on the presence of organic compounds within a sample and can inform decisions on water use and treatment. Traditional oxygen demand measures are time consuming and require the use of harmful reagents. TiO₂-based photoelectrochemical oxygen demand (PeCOD) methods offer a faster, more efficient, and accurate alternative to traditional analysis processes. These methods use TiO₂-mediated photoelectrocatalysis (PEC) to oxidize organic contaminants. This paper reviews the recent synthesis methods of TiO₂ nanomaterials with respect to electrode preparation in COD sensors, fundamentals of TiO₂ photo/photo-electrocatalysis, TiO₂ based PeCOD sensors, and PeCOD sensor system cell design. PEC combines photocatalysis with electrochemical methods, which result in improved photocatalytic performance in a variety of applications. TiO₂ based PeCOD sensors are promising due to their intrinsic low cost, non-toxicity, chemical stability, and availability in sensing applications. Here in this paper, an innovative PeCOD sensor system cell design system is demonstrated. This review paper aims to provide a scientific and technical overview of TiO₂ PeCOD sensor systems implementable for large-scale environmental, soil, and gas sensing applications.

Contents

1. Introduction	2
2. COD sensors	2
3. Fundamentals of TiO ₂ photocatalysis and TiO ₂ photoelectrocatalysis	3
3.1. TiO ₂ photocatalysis mechanism	3
3.2. TiO ₂ photoelectrocatalysis mechanism	4
3.3. Determination of COD by Thin-Layer photoelectrochemical cell	5
4. Industrial TiO ₂ PeCOD® system Design, fabrication and testing	5
4.1. Microfluidics design	5
4.2. Control of operation	8
4.2.1. Calibration of a sample with known COD	8
4.2.2. Sample measurement of a sample with an unknown COD	9
5. TiO ₂ based PeCOD sensor studies	9
6. Synthesis of TiO ₂ nanostructures	10
6.1. Electrochemical anodization	10

* Corresponding author.

E-mail address: bbastuga@uwaterloo.ca (B. Bastug Azer).

<https://doi.org/10.1016/j.jelechem.2022.116466>

Received 23 March 2022; Received in revised form 16 May 2022; Accepted 25 May 2022

Available online 30 May 2022

1572-6657/© 2022 Elsevier B.V. All rights reserved.

6.2.	Hydrothermal synthesis	11
6.3.	Synthesis of TiO ₂ inverse opal structure	12
6.4.	Electrospinning	12
6.5.	Chemical vapor deposition (CVD)	13
6.6.	TiO ₂ based nanocomposites	13
6.7.	TiO ₂ electrode preparation	13
7.	Conclusions	14
	Declaration of Competing Interest	14
	Acknowledgments	14
	References	14

1. Introduction

The past century has seen drastic increases in population and industrialization, resulting in a proportional increase in demand for water and water purification technologies. The discovery of the Honda - Fujishima Effect and related technological advances in photo-electrocatalysis (PEC) gather significant interest as a pathway to meet unprecedented needs [1,2]. Developments in PEC technologies for water purification align with increasing standards and demands [3] for wastewater management to limit contamination and secure potable water sources. These factors have generated demand for rapid, accurate, and environmentally friendly wastewater monitoring. Poorly managed wastewater can limit the available drinking water, spread disease, and present heightened ecological threats.

The degree of organic and biological contamination in water contributes to the chemical oxygen demand (COD) and biological oxygen demand (BOD) respectively. Although COD and BOD are industrially standardized measurements, their evaluation has not traditionally been rapid, accurate, or environmentally friendly. Typical COD evaluation requires the use of strong oxidizers (potassium dichromate) and acids (sulfuric acid), and the process is not always accessible due to the significant skill, equipment, and time requirements. Although standard BOD measures do not require dangerous reagents, more time is required, and the measurement error is typically between 10 and 20% [4-6]. Photoelectrochemical oxygen demand (PeCOD) offers an alternative that can be performed swiftly, accurately, and without the use of toxic or harmful reagents.

TiO₂-based photo-electro-catalytic COD determination has significant advantages over standard COD methods due to titania's native high stability, non-toxicity, abundance, and strong oxidation capability [7,8]. However, the system must be carefully designed to obtain high performance [7]. There are three primary phases associated with TiO₂, anatase (E_g = 3.2 eV), rutile (E_g = 3 eV) and brookite [9]. In ambient conditions, the rutile phase is thermodynamically stable while the anatase and brookite phases will revert to rutile at high temperatures. Due to difficulties in synthesis and limited photocatalytic performance, brookite is the rarely reported phase of TiO₂ [10]. This is, however, a bulk behavior; at TiO₂ surfaces, the anatase phase is thermodynamically preferred due to the lower overall surface energy. Although anatase has higher PEC performance, mixed-phase systems outperform single-phase titania crystals. This results in significant complications at the nanoscale; processes designed to generate bulk phase compositions will no longer hold for nanomaterials [11]. Consideration, then, must be made for both the volume-to-surface area ratio and rutile-to-anatase phase ratio when designing synthesis processes [12,13].

TiO₂ PEC occurs when the photoanode, under some external bias, is illuminated by a UV light source. The absorbance of TiO₂ can differ depending on properties such as morphology, thickness, and annealing temperature, but in general it is photoactivated by wavelengths in the UV region [14-16]. The UV light source excites valance band electrons to the conduction band, producing electron/hole pairs, termed excitons. These excitons can then be separated to generate surface holes

and free electrons. When the TiO₂ surface is exposed to an aqueous solution, the holes can interact with oxygen and water species to form an assortment of oxygen radicals (i.e., •O, •OH, •O₂). The corresponding electrons undergo reduction reactions, commonly H⁺ is reduced to H₂ by the excited electrons or are collected and removed to some external circuit [17]. In the presence of oxidizable species, the oxygen radicals will, in general, decompose organics to CO₂, H₂O and mineral acids. This well-documented mechanism is the fundamental principle behind the PeCOD system. When the generated holes are consumed in oxidative reactions, an excess of electrons will be preserved. By collecting and measuring these charges the demand for oxidation in a sample may be calculated [18,19].

PeCOD is a well-established method [20] for the determination of organic species in water. This system has been used in several applications such as industrial & municipal wastewater, [21-24], pulp, paper, food, beverage, and drinking water applications [25,26]. Several parameters for PEC cell design play significant roles in the efficiency and performance of PeCOD devices. The cell surface-area-to-volume ratio determines the time scale of a specific cell reaction due to diffusion-limited behaviors. The microfluidic design controls in particle size effects (clogging, settling, flow rates, etc.) depending on the aims and priorities of the system. The surface roughness and sealing of the cell also play a role in the performance and expected error of PeCOD measurements. Given that a calibration stage is necessary, PeCOD systems require a high degree of reproducibility in their design; therefore, the operation parameters of this system will be discussed with respect to the resulting performance and possible areas of concern or improvement.

Particular attention is needed to optimize the photoanode material morphology in PeCOD systems. Several factors are commonly at work; a higher surface-area-to-volume ratio will result in more surface sites for oxidation reactions while free particles/porous films will permit more solution-catalyst interactions and fixed-films are more easily recovered [27]. Grain boundaries will hamper electron collection but may be necessary to permit a high surface-area-to-volume ratio [28,29].

Other works only touch on performance parameters and design considerations for a reaction cell in this application. In this review, a detailed discussion of the design and optimized operation of an industrial PEC device and the effect of different TiO₂ production techniques and structures on COD determination will be analyzed as a complete system for the first time to highlight the importance of the TiO₂ based PeCOD system.

2. COD sensors

Oxygen demand has been gathered interest as a key parameter to represent the quality of water and wastewater [30]. In short, there are two standard analytical methods used to determine the quality of water sources; COD represents the degree of organic pollution, and BOD is a calculation of the oxygen consumed in microbial degradation processes [31]. Especially in heavily polluted water sources,

COD is preferred for determining the oxygen demand of organics. The oxygen demand is calculated with this method by analyzing the oxidative degradation in the presence of strong oxidizing agents. Traditional COD methods are generally performed using dichromate as a primary oxidizer.

However, these traditional techniques have several disadvantages [32]. The analysis is time-consuming and requires expensive, corrosive, and toxic reagents, such as Ag_2SO_4 , HgSO_4 , and $\text{Cr}_2\text{O}_7^{2-}$. Because of these drawbacks, the dichromate standard COD method is not desirable for large-scale environmental and industrial assessment applications. As discussed, modern techniques such as electrochemical techniques and photocatalytic methods have been developed as replacements and have become promising methods in the COD detection field. Specifically, oxidation by UV-activated photocatalytic materials has become the preferred operating principle for research into the COD measurement systems [33,34]. TiO_2 is often the most dominant material due to its strong capability to oxidize almost any organic compound under illumination. These properties have been the primary driving factors for the attention given to TiO_2 -based photocatalytic/PEC sensors [6]. TiO_2 COD sensors are highly attractive due to their non-toxic, inexpensive, and biocompatible nature coupled with a strong oxidizing performance, and high photostability [35].

3. Fundamentals of TiO_2 photocatalysis and TiO_2 photoelectrocatalysis

3.1. TiO_2 photocatalysis mechanism

TiO_2 is an *n*-type semiconductor with wide bandgap energy [36], which tends to have electron-donating oxygen vacancies. When energy of photons greater or equal to the bandgap energy (3.2 eV for anatase and 3.0 eV for rutile), electrons from the valance band are excited to the conduction band while holes are left behind in the valance band. This photoexcitation process is shown in Equation (1), Fig. 1 [37].

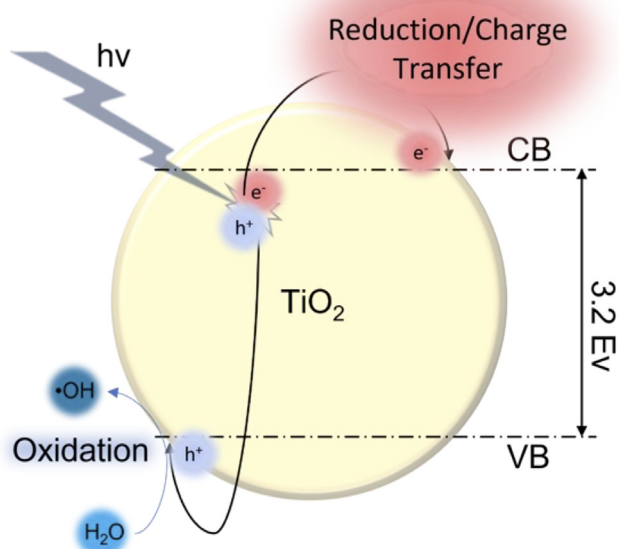


Fig. 1. Schematical representation of energy bandgap diagram and photocatalytic process on a TiO_2 particle.

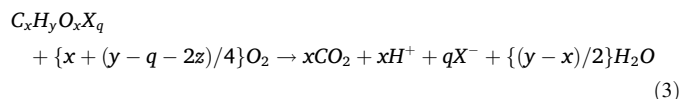
The formation of a free electron at CB and a paired hole at VB is referred to as an electron/hole pair or exciton, while the inverse reaction of Equation (1) is known as recombination. The holes, created by Equation (1), also called photoholes, have a powerful oxidation capability (+3.2 V) and are able to oxidize a wide range of organic compounds in water [38-40]. The oxidation is performed via two primary pathways.

In the first pathway, oxidation happens at the surface of TiO_2 . Organic species are adsorbed onto the surface of TiO_2 , and photocatalysis may take place [41-43].

The second pathway utilizes the presence of the surrounding liquid medium. Water is oxidized by the generated photoholes, which leads to a heightened concentration of hydroxyl radicals ($\bullet\text{OH}$), shown in Equation (2). Although oxidation reactions can produce a variety radical species, the hydroxyl radicals are the primary oxidizing agents. These hydroxyl radicals behave as strong oxidizers and are known to be able to oxidize a large variety of organic compounds [44-47].



In order to obtain efficient mass transport, the photocatalytic degradation of organic compounds (e.g., $\text{C}_x\text{H}_y\text{O}_z\text{X}_q$) is commonly performed using a suspension of TiO_2 particles. The complete oxidation reaction (using either of the reaction pathways aforementioned) can be summarized by Equation (3) [34]:



However, there are two main handicaps associated with TiO_2 photocatalytic colloidal slurry suspension systems. The system introduces the need for a costly and challenging post-treatment to separate and recycle the TiO_2 catalysts from a liquid reaction media. This is the most important barrier to practical applications [48,49]. Many propositions to overcome these challenges have been tested, the most popular being the immobilization or deposition of TiO_2 on some other substrates such as titanium, organic polymers, silicon, etc. [50,51].

The second drawback is the fact that the electron-hole recombination reaction, which is the reverse reaction of the electron-hole dissociation reaction, given in Equation (1), of TiO_2 occurs rapidly. This is also an indicator of a low or competitively unfavorable photocatalytic degradation mechanism on the TiO_2 surface [41,52]. The recombination reaction is given in Equation (4).



In order to improve the photocatalytic degradation rate, the recombination of electron-hole pairs (Equation (4)) should be limited. This can be achieved by physically separating the photogenerated electrons and holes, which is easily and commonly achieved by reducing the number of electrons in the conduction band [18]. Electron removal is commonly facilitated with the use of a potential bias applied across the TiO_2 , typically used an effective means of separating the photoelectrons and photoholes. This can result in a significant improvement of the photocatalytic efficiency of TiO_2 . This mechanism will be further addressed in section 3.2.

3.2. TiO_2 photoelectrocatalysis mechanism

The two main drawbacks of photocatalysis systems can be fixed by the immobilization of TiO_2 on a conducting substrate and the application of an electric bias. In TiO_2 PEC systems, TiO_2 nanoparticles are often fixed onto conducting substrates; this forms a TiO_2 film electrode, called a photoanode, typically used as a working electrode. An appropriate potential bias is applied on the working electrode [41,42,53-55], which results in the transfer of photoelectrons through an external circuit. As seen in Fig. 2, with the application of an external

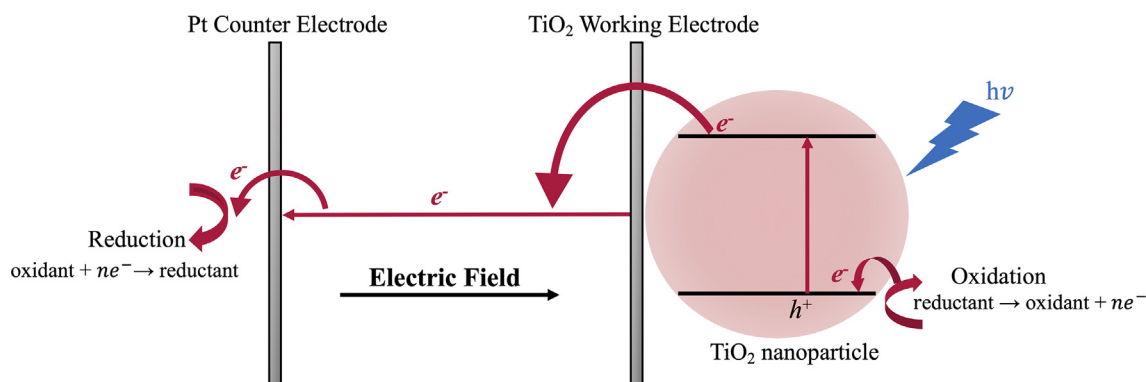


Fig. 2. Schematic representation of photoelectrocatalytic process at a TiO₂ photoelectrode.

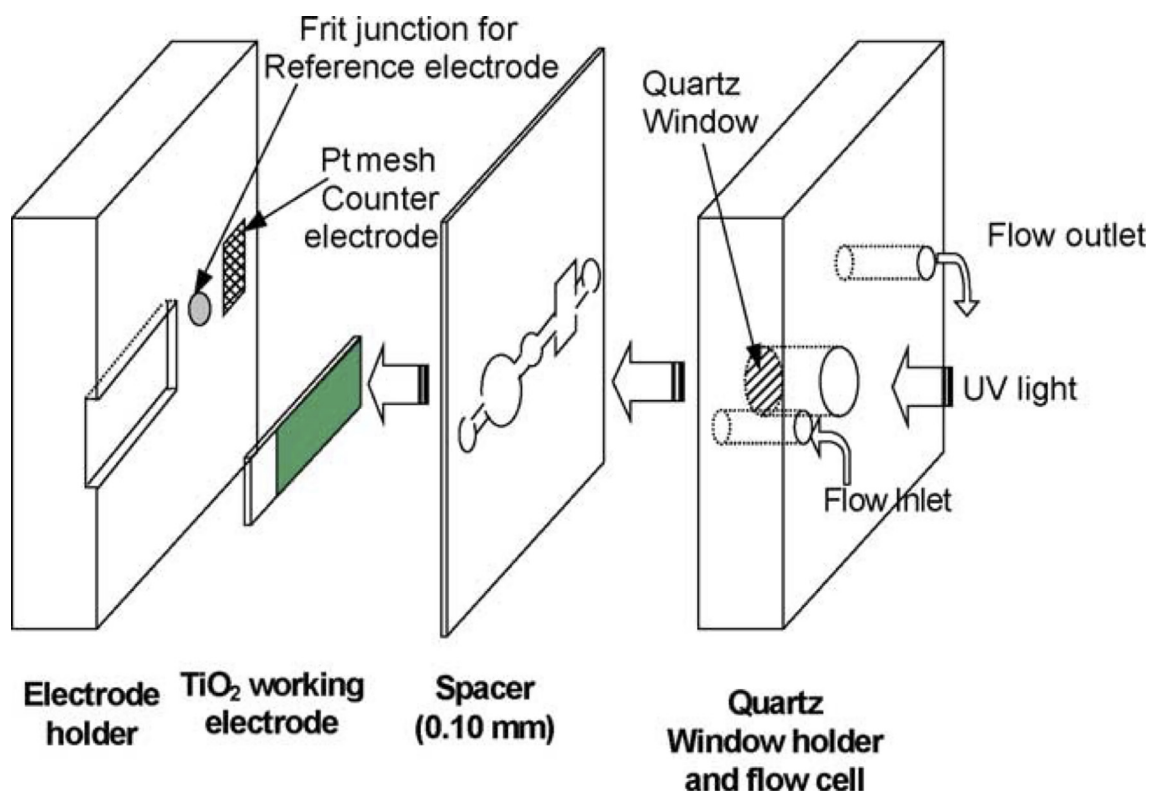
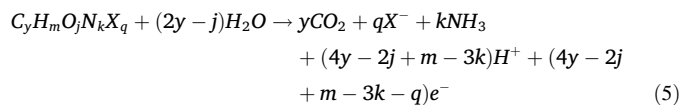


Fig. 3. Schematic representation of the thin-layer photoelectrochemical cell [41]. (Reprinted from Zhang et al. 2004. Copyright (2004), with permission from Elsevier.).

bias, the photogenerated electrons are forced to pass through the external circuit and delivered to an auxiliary electrode [36,56,57]. Due to the application of a potential bias, reduction reactions occur at the auxiliary electrode while the oxidation reactions take place at the working electrode, i.e. the TiO₂ photoanode [58]. This electric potential not only physically separates the oxidation and reduction reactions, thereby suppressing the recombination of photoelectrons and photoholes (Equation (4)), and improving the photocatalytic oxidation efficiency, but also provides a pathway to monitor the photocurrent for the determination of the concentration of organic compounds [41].

Because of the strong oxidation power of the photoholes for oxidation at the TiO₂ electrode, the following stoichiometric oxidation reaction of organic compounds can be determined [41]:



Here the elements are represented by their atomic symbols and X represents some halogen atom. The stoichiometric number of atoms in some organic compounds are represented by y , m , j , k , and q . Therefore, $(4y - 2j + m - 3k - q)$ will correlate to the oxidation number (n). This oxidation reaction is regularly used to determine the COD. There are primarily two analysis methods, probe type TiO₂ photoanodes and thin-layer photoelectrochemical cells [31,41,59-61]. This paper is focused on the COD determination in thin-layer photoelectrochemical cells.

3.3. Determination of COD by Thin-Layer photoelectrochemical cell

Zhao et al. [31] invented, designed, and developed the first thin-layer photoelectrochemical cell (Fig. 3) using TiO₂ photoanode for photoelectrochemical determination of COD values in water, which became known as the PeCOD method [41,42]. This has since been patented in partnership with Aqua Diagnostics Pty Ltd, Australia [62]. The thin-layer photoelectrochemical cell was developed to shorten the degradation time and maximize the degradation efficiency [41]. Their work demonstrates two modes of thin-layer three-electrode photoelectrochemical cell operation: a stop-flow exhaustive oxidation mode and a continuous-flow partial oxidation mode [60].

Under constant UV illumination, the light source ideally has a peak wavelength of 365 nm, at which the TiO₂ demonstrates a set photocurrent response, visualized in Fig. 4. Here i_{blank} (solid line) corresponds to current obtained from the PEC oxidation of water, while i_{total} (dashed line) represents the PEC oxidation of water and organic compounds present, i.e. i_{total} consists of two components, PEC oxidation of water (i_{blank}) and the PEC oxidation of any organic compounds (i_{net}). Both solutions require a stabilizing electrolyte (LiNO₂), however, a detailed discussion on the electrolyte impact is beyond the scope of this work. Therefore, i_{net} is calculated as follows (Equation (6)) [31]:

$$i_{net} = i_{total} - i_{blank} \quad (6)$$

By integrating the photocurrents i_{blank} and i_{total} with respect to time, the blank charge Q_{blank} and total charge Q_{total} can be calculated respectively (Equation (7)) [31].

$$Q = \int idt = nFVC \quad (7)$$

where i is the current generated by PEC oxidation, n is the number of electrons transferred due to the PEC oxidation (i.e. oxidation number given by $(4y - 2j + m - 3k - q)$ in Equation (5)), F , V , and C are the Faraday constant, volume of reactor cell and molar concentration of the sample, respectively. Q_{net} , net charge obtained by oxidation of organic compounds (the shaded area in Fig. 4), can be calculated by subtracting Q_{blank} from Q_{total} , which is shown in Equation (8) [31].

$$Q_{net} = Q_{total} - Q_{blank} \quad (8)$$

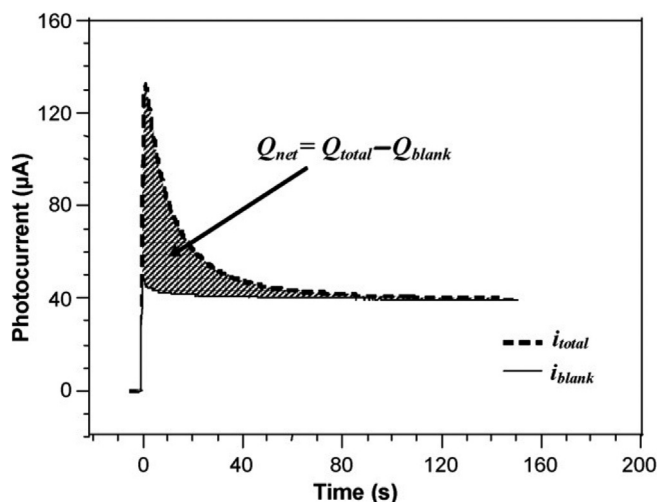


Fig. 4. Photocurrent responses of a blank solution (solid line, i_{blank}) and a sample containing organic compounds (dashed line, i_{total}) in a photoelectrochemical thin layer cell, the shaded area indicates the complete oxidation from the charge, which is called Q_{net} [41]. (Reprinted from Zhang et al. 2004. Copyright (2004), with permission from Elsevier.).

Under exhaustive oxidation mode, the calculated net charge, Q_{net} , is used as a direct measure of the total number of electrons obtained from the PEC mineralization of all compounds in a sample. As shown in Equation (9), four electrons are transferred per oxygen molecule; the measured Q_{net} value can then be converted to some equivalent O₂ concentration, i.e. oxygen demand. The equivalent COD value can be calculated as given in Equation (10) [31].



$$COD(mgL^{-1}O_2) = \frac{32000}{4FV} Q_{net} \quad (10)$$

4. Industrial TiO₂ PeCOD® system Design, fabrication and testing

In this section, an industrial TiO₂ PeCOD system, PeCOD®, is investigated in terms of design and fabrication considerations with illustrating testing procedure. As explained in section 3.2, the two main drawbacks of TiO₂ photocatalytic systems, the recombination of photogenerated electron-hole pairs and the separation of TiO₂ nanoparticles from the reaction media, are partially improved by fixing the active TiO₂ onto a conductive substrate, under an electric field. The application of an electric field is not only effective for separating oxidation and reduction reactions but also enables the measurement of generated current, which can then be correlated to COD.

The aim of the system is to measure the COD of a set of solutions by counting the electrons associated with oxidation (Equation (5)) for wastewater and drinking water applications. The measured net charge is proportional to COD as shown in Equation (10); this linearity allows the system to analyze solutions up to 300 mg·L⁻¹. In this system, samples are mixed with a fixed ratio of a LiNO₂ electrolyte solution to ensure reliable electrical conductance as some electron transfer from the solution to an electrode is required for PeCOD determination, seen in Fig. 2. The ratio of electrolyte to sample solution is called the dilution factor. In this system, samples up to 15,000 mg·L⁻¹ may be analyzed with a maximum dilution factor of 50.

To calculate COD, sensing cell volume, V , and net charge, Q_{net} , are required as illustrated in Equation (10). These terms are discussed in the following sections as microfluidics and control, respectively.

4.1. Microfluidics design

Due to the micro-scale sample size and the sensitivity of the cell to variations in the operating conditions, concerns and methodologies relating to the microfluidic operation and performance must be considered. Two types of solutions are analyzed sequentially in each operation, called the blank and sample solutions, to calculate Q_{net} as shown in Equation (8). The blank solution is a mixture of DI water with some electrolyte, while the sample solution is prepared by mixing an unknown sample with electrolyte at the same dilution factor, depending on the anticipated COD range. The schematic of the microfluidics circuit is given in Fig. 5.

This system employs three valves and a pump; the first valve, termed the selector valve, is utilized at the inlet side to analyze blank and sample solutions sequentially. Then the switch valve, normally off for sealing, is activated simultaneously with the pump to introduce the solution to the system. The third, flush valve, discharges the excess solution to prevent electrode wear and increase the sensor lifetime. After analysis, the pump discharges the accumulated solutions as waste. All operational elements are connected via microfluidic channels, while targeted oxidation reactions occur in the sensing cell, driven by an active TiO₂ electrode and UV illumination with a 365 nm wavelength LED source.

Ideally, all the solution introduced to the sensing cell is oxidized and contributes to the COD calculation, as illustrated in Equation (10). However, there are some limitations that cause a decrease in oxi-

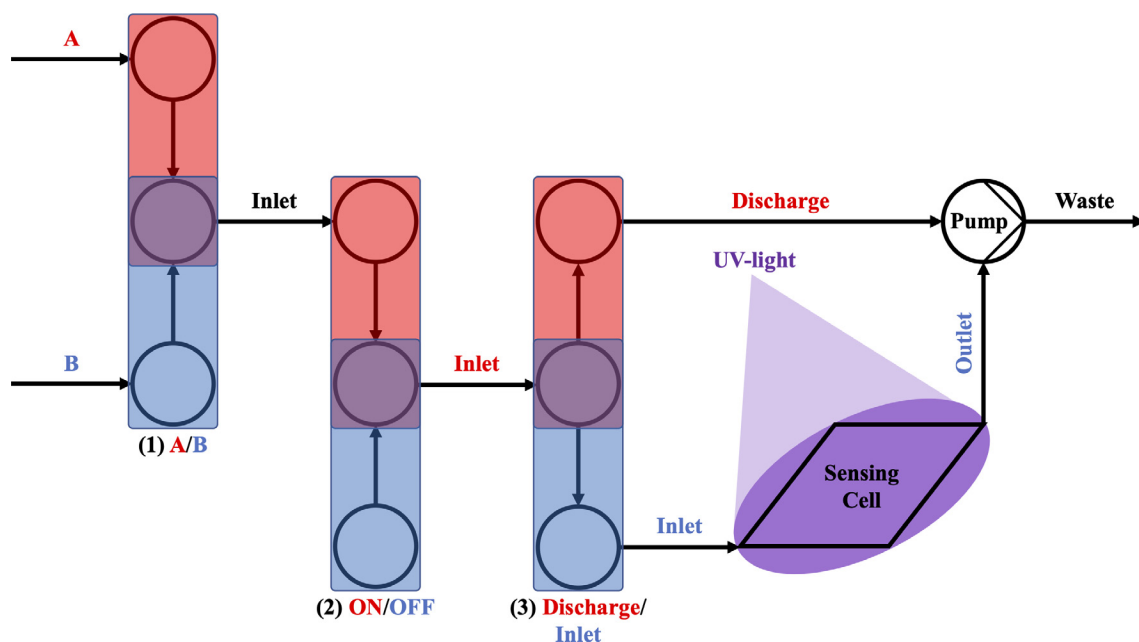


Fig. 5. The schematic representation of microfluidics circuit; here A is the blank and B is the diluted sample.

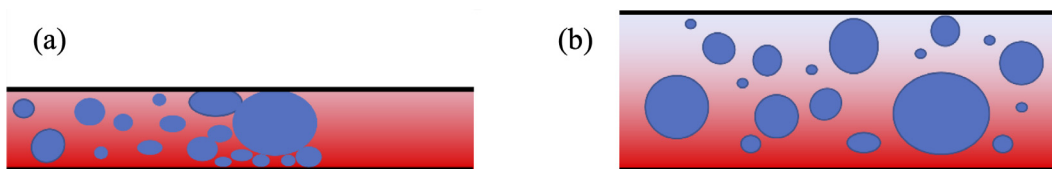


Fig. 6. Illustration of thickness on performance. Red indicates higher electron-hole density. A thinner sensing cell (a) has faster oxidation rate with higher change of particle stuck while thicker one (b) has slower oxidation rate with lower chance of particle stuck. (For interpretation of the references to color in this figure legend, the reader is referred to the web version of this article.)

dation. The first concern is due to the finite thickness. As the distance from the electrode increases, the degree of photocatalytic oxidation

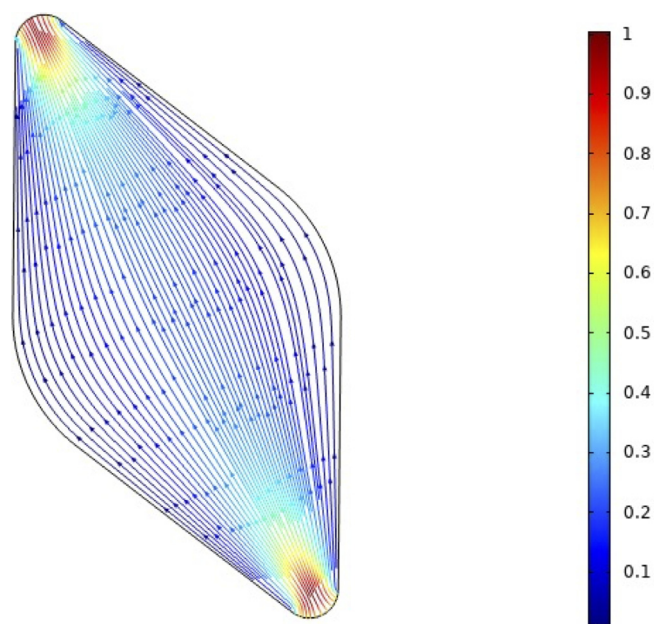


Fig. 7. Velocity streamlines of PeCOD® sensing cell with FEM analysis (scale bar values are normalized).

decreases due to the diffusion-limited dependence of the oxidizing species interacting with spatially separated organic contaminants. To stabilize the reactants and encourage charge transfer, the electrical conductivity of the solution is increased by introducing preferred electrolytes into the solution. Therefore, the thickness of the sensing cell should be as small as possible to minimize the dependence on diffusion and to increase the overall oxidative performance. However, it should be also thick enough so that large particles don't get stuck inside. To address this concern, filtration is done before each analysis to remove excessively large particles. Fig. 6 illustrates the effect of sensing cell thickness on the operation.

The filter size should be chosen for sensing cell thickness, otherwise, large particles could stick in the sensing cell.

A second concern arises due to the no-slip boundary condition at the solid-liquid interface, which can result in excess solution in the cell after rinsing. This excess will change the effective cell volume and, in some cases, can contribute unexpected species to the COD measurement. To have a linear relationship between COD and Q , this excess must be removed to minimize error in the volume and COD calculations. To ensure these factors are negligible, a finite element method (FEM) analysis of microfluidics system has been investigated when the pump is active. Velocity streamlines of designed sensing cell is shown in Fig. 7.

Any vortex and eddies cause leftovers during discharge therefore it is important to have continuous streamlines from inlet to outlet that are located bottom and top in Fig. 7, respectively. No slip boundary condition applies at outer walls of the sensing cell, shown as black color, and geometry of this wall plays a huge role in velocity stream-

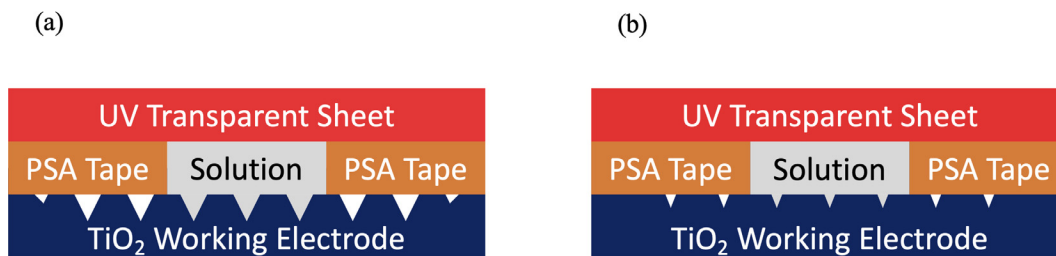


Fig. 8. Cross-sectional view of sensing cell. Higher surface roughness (a) has more surface area but low sealing performance while flatter one (b) has less surface area with better sealing performance.

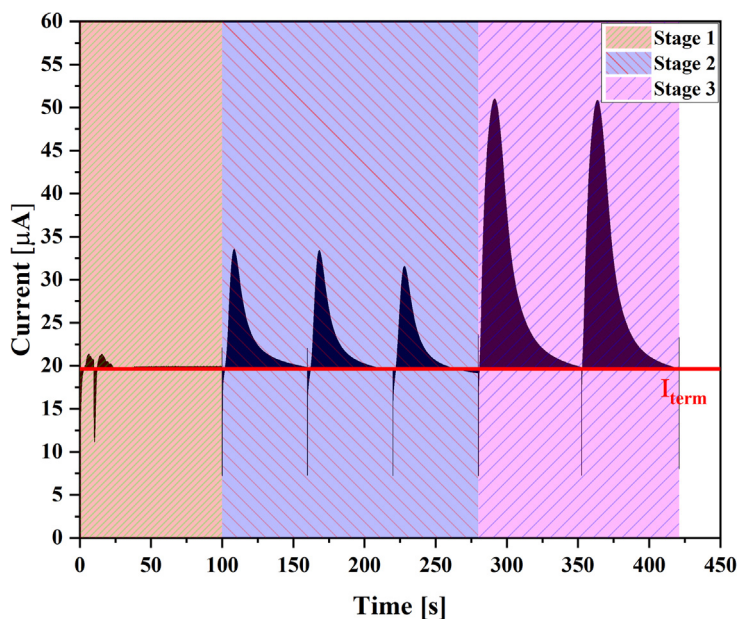


Fig. 9. An example calibration curve.

lines. Sharp edges in outer wall cause vortex and eddies in velocity streamlines and to minimize the leftovers during discharge, outer wall of sensing cell is constructed with round edges instead of sharp edges.

The final consideration is the overall sealing of the cell housing. It is well reported that, as the surface roughness of the electrode increases, the effective surface area increases, and the photocatalytic performance improves [63]. However, higher surface roughness introduces sealing problems [64] as shown in Fig. 8.

The sealing performance plays a huge role in the experimental repeatability. Poorly sealed cells produce no current response and represent the main source of error in these systems. Although a higher surface roughness of the electrode offers improved performance, minimal surface roughness is recommended in commercial usage for repeatability and smooth operation.

4.2. Control of operation

Throughout the fabrication and design process, some consideration must be taken to determine the specific methodologies and concerns associated with the operation and precise control of the sensing device. The fundamental goal of the sensing device is to calculate Q_{net} using Eqs. (6–8). The collected current passing through the electrode is calculated by connecting a series resistor at the end of the electrochemical circuit and measuring the voltage on top of it, via ohms law. The theoretical ratio between COD and Q_{net} , defined as the theoretical M value ($M_{theoretical}$), can be calculated as $0.021 \text{ COD}/\mu\text{C}$ using

the Equation (10), as the specific volume of our system is $3.88 \mu\text{L}$. Although the microfluidic design is designed to achieve complete oxidation, there's still some variation between $M_{theoretical}$ and the actual ratio, M , between COD and Q_{net} due to the volume term in Equation (10). Therefore, for accurate measurements, M should be measured experimentally with a calibration process.

4.2.1. Calibration of a sample with known COD

Calibration is done with some samples of a known COD to calculate M , which relates COD to the total charge collected. Various calibrants may be used, depending on the desired sensitivity range. The reported results are calibrated to a standard, termed the calibrant solution, which is a mixture of DI water, lithium nitrate, sorbitol, and silver nitrate with a known COD of $20 \text{ mg}\cdot\text{L}^{-1}$ and a sucrose concentration of 20 mol/L . A standard calibration run is shown in Fig. 9.

The calibration process is split into three stages. All three stages consist of a liquid sample and some photo-illumination intensity; in this setup, only the light intensity is a controlled parameter. The first stage, from 0 to 100 s, is the equilibrium adjustment phase. A mixture of DI water and lithium nitrate, termed the blank solution, is pumped into the system. The LED intensity is adjusted to maintain a set steady-state current, I_{term} , associated with water hydrolysis. After 100 s of this control region, the LED current is held at a predetermined constant value for the remaining stages. This input LED current is typically manipulated to set the generated output I_{term} at $20 \mu\text{A}$ which corresponds $0.41 \mu\text{A}/\text{mm}^2$ current density. I_{term} was set experimentally,

and it's been observed that higher I_{term} causes earlier saturation in long term and results shorter lifetime while lower limits Q_{net} and decreases the sensitivity.

The current required to do so over repeated calibration analysis runs is shown in Fig. 10.

As shown in Fig. 10, a larger system input, LED current, is required to have the same output (I_{term}) over the lifetime of the sensor. The main reason is the loss of active material, TiO_2 , due to aging and wear. At failure, the color of the ITO-coated glass slide changed from opaque and dark to transparent; this is strongly indicative of wear-off due to interaction with the solution and prolonged photocatalytic activity. At around 1100 runs the LED current reaches saturation, around 465 mA, at that point the system cannot provide enough input to achieve the desired output.

Variation in the system output, I_{term} , in the long-run calibration analysis is shown in Fig. 11. As indicated, after input saturation, the system output cannot reach the set-point I_{term} . On the other hand, in the non-saturation regime, the control stage works properly to maintain the desired system output within some small variation.

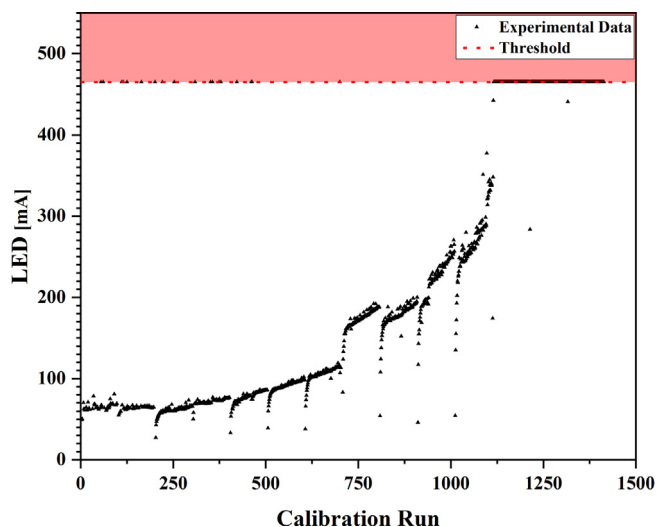


Fig. 10. LED Current with respect to calibration run count.

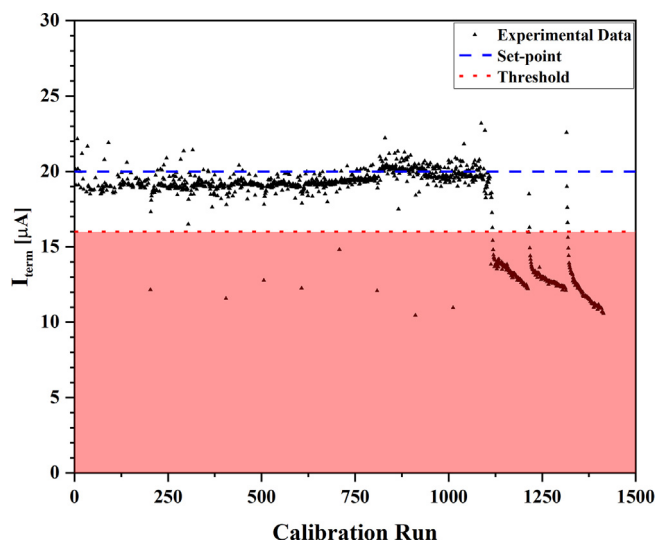


Fig. 11. I_{term} variation in long-run calibration analysis.

The second stage of the calibration analysis is termed blank measurement. The goal is to calculate the charge generated by the hydrolysis of water, denoted as Q_{blank} . Again, the blank solution is pumped into the system and the response is measured. Q_{blank} is calculated by integrating the area of the response curve over the I_{term} line, averaged over three repeated measurements. Variations in the Q_{blank} values in a long-run calibration analysis are shown in Fig. 12.

The desired Q_{blank} range for this system of calibration ranged from 50 μC to 300 μC , depending on the photocatalytic efficiency, sample, and sensor characteristics. Aside from experimental errors, this condition is reliably met over the full sensor lifetime.

The third and final stage of the calibration is the sample measurement. The aim is to calculate Q_{total} associated with both the hydrolysis of water and the oxidation of organic compounds. The sensor response is then recorded; from this, the area is calculated by integrating between the response curve and the I_{term} line. This is done twice and averaged in order to produce a more reliable result. Variations in Q_{total} over the lifetime of a sensor in a long-run calibration analysis are shown in Fig. 13.

Since the aim of the calibration process is to calculate the M value, the net charge due to oxidation of organic compounds is required. It

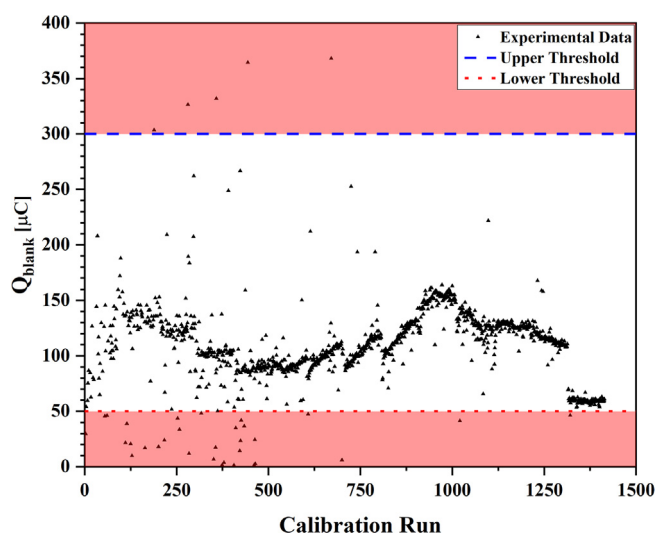


Fig. 12. Q_{blank} distribution in long-run calibration analysis.

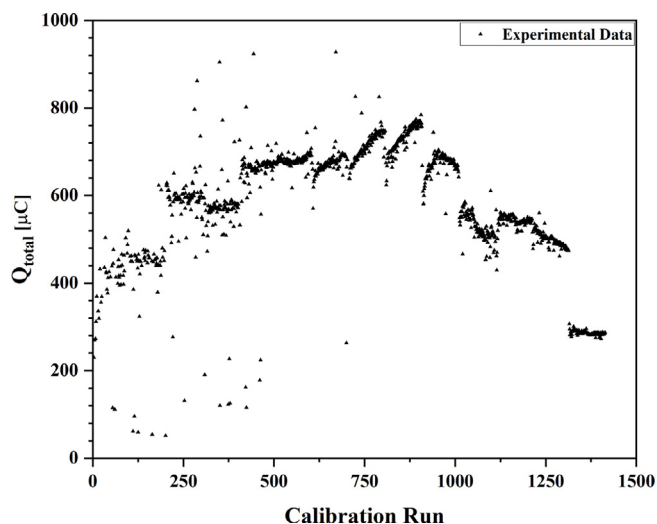


Fig. 13. Q_{total} behavior in long-run calibration analysis.

can simply be calculated by subtracting Q_{blank} from Q_{total} as shown in Equation (8). Variation of Q_{net} in long-run calibration analysis is shown in Fig. 14.

As explained above, there is a wide variation in Q_{net} due to the volume term of Equation (10). A control mechanism and calibration process are required for accurate and sensitive COD measurement. It is clear that the system can collect enough charge to relate the COD of a calibrant solution with Q_{net} up until 1300 runs and successfully calibrate itself. The final step in the calibration process is to divide the COD of a known solution, here $20 \text{ mg}\cdot\text{L}^{-1}$, by Q_{net} to determine the M value. Variation in M value over the lifetime of a sensor in a long-run calibration analysis is shown in Fig. 15.

As mentioned earlier, there is often a significant deviation between experimental and theoretical M values. The main reason for this variation is the volume term from Equation (10). Typically, an ideal volume is assumed with the expectation that all solutions in the sensing cell are oxidized by the end of the PEC process. In practice, due to the finite thickness of the sensing cell, there is some distance from the top of the cell and the TiO_2 electrode. As the distance increases the photocatalytic effect decreases. Therefore, a decrease in oxidation in the sensing cell is expected due to diffusion limitations governing

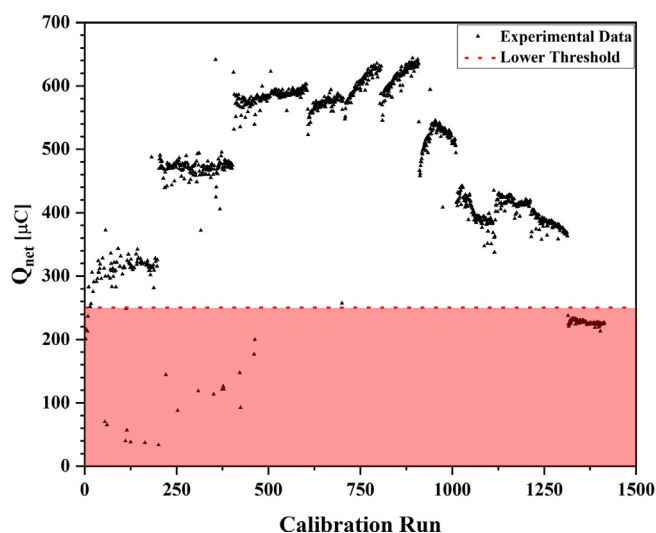


Fig. 14. Q_{net} behavior in long-run calibration analysis.

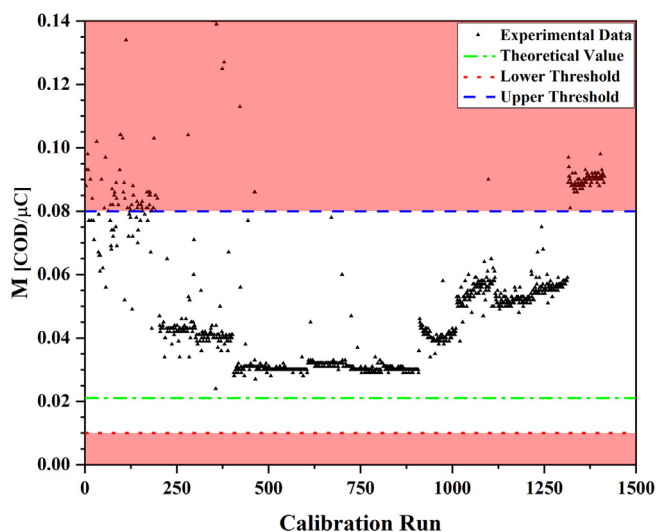


Fig. 15. M value trends in long-run calibration analysis.

some regions of the sample cell. This is associated with a higher experimental M value than theoretically predicted. From the theoretical calculations, the volume is defined from the surface area and thickness of the sensing cell. In practice, there is surface roughness due to the uneven TiO_2 coatings on the ITO/glass substrate. Additional concerns arise from the practical production of these sensing cells; specifically, from the polymer used to set the boundary of the sensing cell walls. Since these polymer tapes are not rigid, there is some strain and deformation arising during the assembly process; this causes some variation in volume. Finally, the solution behaves as if there were non-slip boundary conditions during the pumping between stages. As a result, some leftover fluid is oxidized repeatedly; this alters the effective volume of the sensing cell, depending on the specific sample composition.

4.2.2. Sample measurement of a sample with an unknown COD

After the calibration is done and an M value is obtained, the system is ready for sample measurements of real samples with unknown CODs. An example of a sample measurement is shown in Fig. 16.

During the sample measurement process, there are only two distinct stages; in the first stage, a blank solution is pumped into the system for stabilization. After 60 s under illumination, a sample of unknown COD is introduced, this process is repeated a second time. Q_{total} is calculated by averaging the area between the curve and the I_{term} line over these two sample measurements. Q_{blank} , from the calibration run, is then subtracted from Q_{total} to find Q_{net} . This value is then multiplied by M to correlate the sample to some sample COD. The system should be calibrated immediately before sample measurements to ensure highly accurate, reproducible, and reliable data.

5. TiO_2 based PeCOD sensor studies

The previous section has broadly covered the industrial usage of PeCOD hardware and software technology. In the following sections, TiO_2 PeCOD sensing systems innovations will be discussed with respect to PEC performance.

Jin et al. [65,66] extensively used TiO_2 electrodes to determine COD values via the measurement of current response in a photo-illuminated system. The primary advantages of this measurement method are lower response times, easier operation, relative cost efficiency, and low environmental impact. In this case, under optimized experimental conditions, a Ti/TiO_2 electrode can measure COD value in a linear range of $50 - 2000 \text{ mg}\cdot\text{L}^{-1}$ with a detection limit reported to

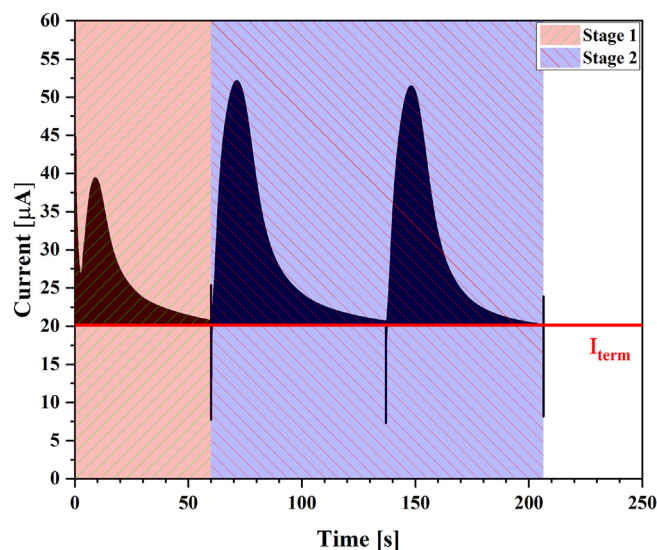


Fig. 16. An example sample measurement curve.

be $16 \text{ mg}\cdot\text{L}^{-1}$ [66]. Significantly improved performance has been obtained through the use of photoelectron-synergistic photocatalysis. Ti/TiO₂/PbO₂ electrodes present a wider range of $20 - 2500 \text{ mg}\cdot\text{L}^{-1}$, with a lower detection limit, $10 \text{ mg}\cdot\text{L}^{-1}$ [65].

Zhao et al. [31] proposed a novel method for determining COD based on photo-electrocatalysis, which they termed as an “exhaustive degradation model”. This group developed a thin layer photoelectrochemical cell which quantifies the sum extent of electron transfer. This direct method does not require the use of a standard for calibration. It utilizes the native high oxidation efficiency and precise charge measurement available to PeCOD systems. Under optimized experimental conditions, a linear range of $0 - 200 \text{ mg}\cdot\text{L}^{-1}$ and detection limit of $0.2 \text{ mg}\cdot\text{L}^{-1}$ have been demonstrated with reported assay times spanned from 1 to 5 min. This method has significant advantages over prior advances; it is rapid, environmentally friendly, and consumes very little reagent.

The PEC performance of TiO₂ can be further through the application of nanostructures; some benefits of tailored structures include better electron-hole separation, electron transfer, and higher surface areas. Mu et al. [67] coated TiO₂ nanofibers on an ITO glass slide and integrated this working electrode in a thin layer PEC reactor for the rapid measurement of COD values. They report a detection limit of $0.95 \text{ mg}\cdot\text{L}^{-1}$ and a working range of $0 - 250 \text{ mg}\cdot\text{L}^{-1}$. They suggest that the TiO₂ nanofibers improved the PEC performance by accelerating the degradation process via enhanced charge separation and diffusion of organics into the nanofiber films.

An extensive selection of fabrication methods has been reported to generate various TiO₂ nanostructures. Zheng et al. [61] fabricated highly ordered TiO₂ nanotube arrays via electrochemical anodization of a Ti sheet. TiO₂ NT sensors show highly efficient photogenerated electron-hole pair separation, which yields improved PEC activity relative to TiO₂ coated nanofilm sensors. This is due to the highly ordered, high aspect-ratio TiO₂ NT structures, which are perpendicular to the conductive Ti substrate. These NT sensor arrays are then integrated into a thin PEC cell, operational in a wide working range of $0 - 700 \text{ mg}\cdot\text{L}^{-1}$ for COD determination. This is a significant improvement in working range compared to other sensors based on TiO₂ coated nanofilms.

6. Synthesis of TiO₂ nanostructures

It is crucial to identify TiO₂ synthesis and manufacturing methods to determine the figures of merit (FOM) for industrial PeCOD sensing devices. Many performance parameters depend on the structure of the TiO₂, specifically sensitivity, lifetime, and the working range; improvements typically involve complex manipulations of a preferential syn-

thesis technique. This section will provide an overview of the recent developments and possibilities regarding synthesis methods of TiO₂.

TiO₂ nanomaterials have been produced by various techniques such as sol-gel, hydrothermal, electrochemical anodization, electrospinning, atomic layer deposition (ALD), chemical vapor deposition (CVD), and physical vapor deposition (PVD). By these methods, several crystal structures of TiO₂ have been prepared: both pressure and temperature play roles in every synthesis method, typically relating to the specific crystal phases present. Nanostructures are preferred due to the fact that larger surface areas and better electron transition states are more accessible at small scales. The geometry of TiO₂ nanomaterials can be zero-dimensional (0-D), such as nanospheres, one-dimensional (1-D), such as nanorods and nanotubes, and even three-dimensional (3-D) nanostructures.

6.1. Electrochemical anodization

In the last 20 years, the fabrication of TiO₂ nanotube arrays (TNA) by electrochemical anodization has been a prominent topic for TiO₂ sensor application studies. The fabrication of TNA was firstly reported by Zwilling et al. [68]. They found that, at a constant anodization potential, TNAs are produced by the anodic oxidation of a titanium substrate in various fluoride-containing electrolytes. Interest surged in the topic following that study. The synthesis, characterization, and application of TNAs have been comprehensively covered and may be broadly categorized into multiple generations of well documented development [69-76]. Fig. 17 illustrates a typical TiO₂ NT array prepared by the anodization of Ti foils using two common electrolytes, which are an acidic fluoride/HF electrolyte and a glycerol/fluoride electrolyte, respectively [77].

It is well documented that the annealing temperature, anodization potential and time, electrolyte type, and pH are the key factors affecting the growth process of TNA materials [78,79]. However, these factors rarely change the phase of the produced TNAs, as anodized TNAs are usually amorphous. Most photocatalytic and sensor applications require crystalline phases of TiO₂ to be effective, therefore, an annealing step is necessary after anodization to increase or manipulate the crystallinity. A strong linear correlation between the wall thickness, diameter of the TiO₂ nanotubes, and the applied anodization voltage has been reported [77,80]. Besides that, the anodization time has a strong effect on the length of TNAs. Interestingly, there are no reports on the relationship between the anodization time and any additional morphological changes [81]. The electrolyte also has a critical effect on TNA formation; several studies show the relation between the nature and age of the electrolyte to the aspect ratio of the produced NTs [78,82]. This is further supported by reports outlining the impact that

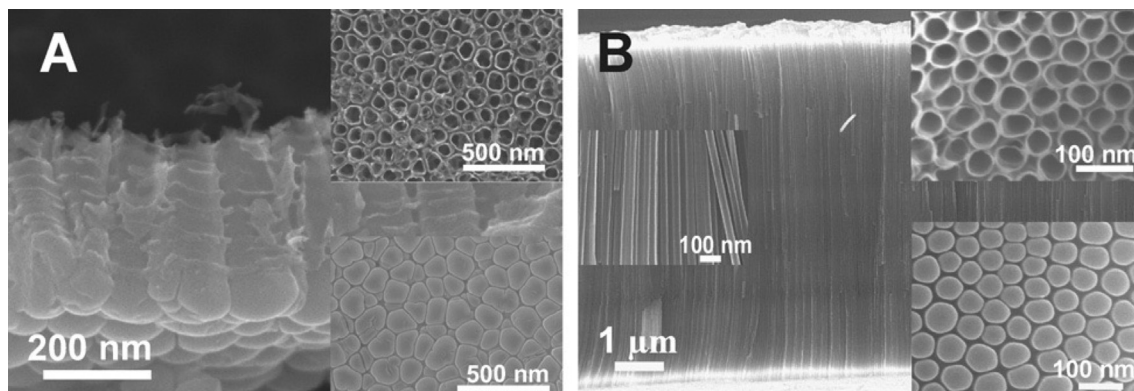


Fig. 17. SEM images of TiO₂ nanotubular structures: a) TiO₂ nanotube arrays produced by the anodization of Ti using acidic fluoride or HF electrolyte (b) long TNAs from Ti anodization using glycerol/fluoride electrolyte [77]. (Reprinted from Macak et al. 2007. Copyright (2007), with permission from Elsevier.).

the temperature and pH of the electrolyte have on TNA formation [76,83].

Zhang et al. [84] successfully developed nanoporous TiO₂ electrode and validated the COD values of actual wastewater and synthetic samples with the PEC method. Their results were in agreement with the standard potassium dichromate COD determination technique; they show a processing time of 1–2 min, a detection limit of 8 mg·L⁻¹ and a linear range of 20–250 mg·L⁻¹. Zhang et al. relate the enhancement in the photoelectrocatalytic activity with the nanoporous configuration, the formation of oxygen vacancies and an improvement in donor density. Si et al. [85] prepared a TiO₂ nanotube array by anodization and subsequently loaded the array with Au nanoparticles. They quantified the COD of organic compounds with known COD values with a detection limit of 0.18 mg·L⁻¹ and a linear range of 1.92 – 3360 mg·L⁻¹.

6.2. Hydrothermal synthesis

The hydrothermal fabrication method is one of the most widely used and well-studied techniques to produce various TiO₂ nanostructures. This technique is especially suited to produce large-scale TiO₂

nanotubes (TNTs) with unique nanotubular structures in the industry [86,87]. The general hydrothermal synthesis is as follows: first, the Ti precursor is dissolved in some aqueous solution (NaOH, HCl, etc.), and the resulting mixture is subjected to a hydrothermal autoclave step to facilitate the conversion from amorphous to nanosized crystalline tubular structures in temperature ranges of 110–150 °C. Then, with a dilute acidic solution or a solvent, the resulting material is washed, dried, and sometimes annealed to produce a nanotubular product [86–89]. It is well known that several factors including the annealing temperature, the nature of the titanium precursor, and the hydrothermal processing time have major roles in nanostructure growth. However, the nature of the aqueous solution used to form the mixture before the autoclave process plays a predominant role in determining the morphology and the final phase. Fig. 18 shows the effect of NH₃ amount both on size and shape of anatase powders which are prepared by hydrothermal treatment [90]. Kobayashi et al. also showed that not only the morphology but also the phase of TiO₂ nanoparticles depend on the concentration of NH₃.

There is a large array of viable morphologies that might be produced via hydrothermal synthesis. Aside from TiO₂ nanotubes, varia-

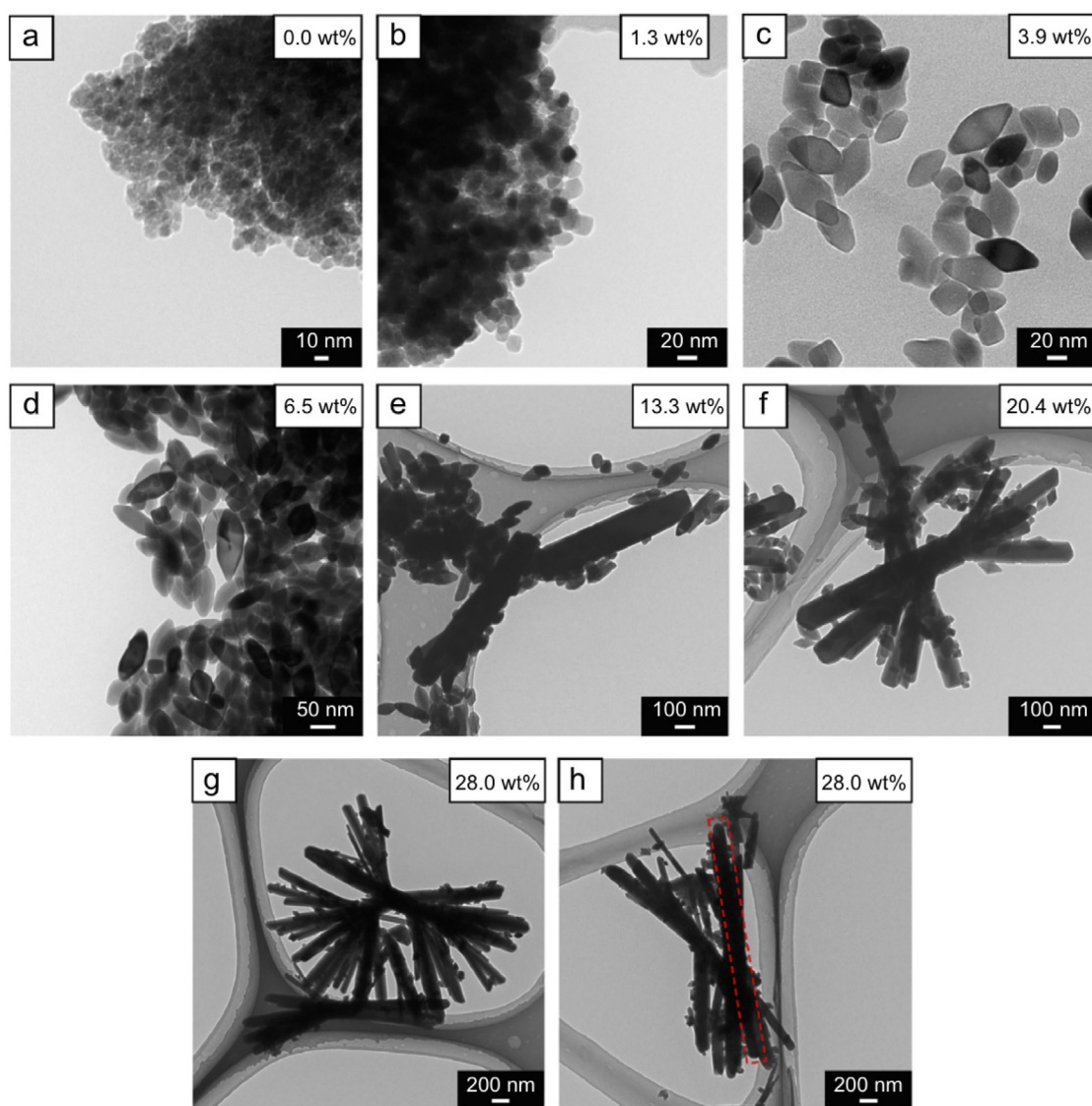


Fig. 18. The effect of concentration of NH₃ on morphology of a mixture of anatase and brookite powders synthesized by hydrothermal treatment of aqueous CPT complex solutions at 473 K for 24 h [90] (Reprinted from Kobayashi et al. 2011. Copyright (2011), with permission from Elsevier.).

tions of nanorods and nanowires of rutile and anatase phases have been shown to be possible target products based on the specific synthesis conditions [91,92].

The hydrothermal reaction time is not only important in terms of structural, optical and morphological properties but also relates to the photoelectrochemical activities of TiO₂ nanorod arrays. Photocurrent density generation from TiO₂ nanorod arrays has a critical correlation with the hydrothermal reaction time owing to an enhancement in the surface wettability and surface roughness, which increase the effective surface area of the arrays [93].

Post treatments are also critical when considering photoelectrochemical applications. Wang et al. [94] formed TiO₂ NTs by the hydrothermal synthesis method and followed by a sulfide treatment. They report a 3.3-fold improvement due to the post-synthesis sulfide treatment. They argue that the improvement is due to the introduction of mesopores on the TiO₂ NTs, which increases the active surface area available for electrochemical activity, optical absorption, and electron transfer rate.

6.3. Synthesis of TiO₂ inverse opal structure

It has been reported that TiO₂ inverse opal structures (TiO₂ IO) demonstrate superior morphological properties compared to other TiO₂ structured materials. There is a significant degree of control with respect to pore size, surface area, and, most importantly, a semi-tailorable photonic bandgap. TiO₂ IOs are generally prepared by the colloidal crystal template method. Commonly, silica (SiO₂) or polystyrene (PS) spheres are used as a template, which is then surrounded by a precursor material and stabilized with several techniques. As a final step, the template is removed either by etching or calcination, depending on the material used. Upon completion, TiO₂ IOs are obtained but may need an anneal step to improve phase uniformity or selectivity [95]. The synthesis of TiO₂ IOs is outlined in Fig. 19 in three steps [95]. It is generally understood that the methodology for producing and introducing the filling material is paramount to the success and functionalization of the IOs. These methods include chemical vapor deposition [96,97], atomic layer deposition [98,99], and the sol-gel method. The most widely used TiO₂ IO preparation is the sol-gel method, as it offers significant advantages such as high purity, good product uniformity, low processing temperature, and, notably, limited demand for expensive instrumentation [100-102].

TiO₂ inverse opals show better photoelectrochemical behavior associated to its better light absorption and improved catalytic oxygen reduction, which is the most important factor for photocatalytic and photoelectrocatalytic performance in TiO₂ inverse opal systems [103,104].

6.4. Electrospinning

Compared to the other listed methods, electrospinning is the simplest and most cost-effective technique to produce 1D TiO₂ structures, especially when producing nanofibers. Traditional electrospinning

equipment has three main components; a high-voltage power supply, the feeding unit, and a collector [105]. The diagram in Fig. 20 shows the general electrospinning equipment setup [106]. 0-D nanomaterials produced by electrospinning generally show worse performance than other methods when comparing PEC applications. The resulting morphology and structures more easily result in the formation of charge carrier recombination sites. For these applications, some research has been done to produce targeted 1D nanostructures using the electrospinning process [105]. To date, the possible microstructures that have been achieved by electrospinning include nano-rice [107], microspheres [108], nanowires [109], and nanotubes [110]. 1-D TiO₂ microstructures produced by electrospinning are noteworthy for their improved performance with regard to the direct electron transfer pathways and fewer grain boundaries, however, nanoparticles typically have a higher surface area than these 1D structures. In order to combine both beneficial aspects, some composite structures of TiO₂ nanotubes and nanoparticles have been produced by electrospinning [111]. For this purpose, the electrospinning technique is preferred for the production of various microstructures.

The morphology control during electrospinning plays an important role in manipulating the photocatalytic and photoelectrocatalytic properties of TiO₂. By tuning these parameters, not only the morphology, but also the crystallinity and the phase ratio can be adjusted. Owing to the higher surface area and particle crystallinity, a targeted degradation performance can be obtained [112]. The hybrid structures formed by electrospinning show an enhanced PEC activity with improved sensitivity and a wide linear detection range [113].

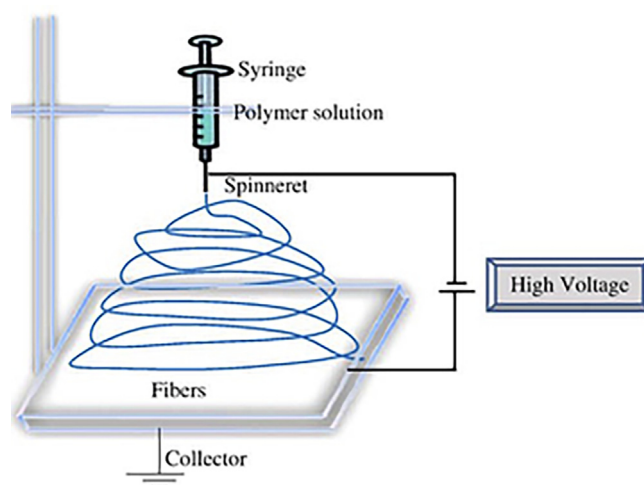


Fig. 20. Representative diagram of electrospinning equipment set up [106]. (Reprinted from Bhardwaj and Kundu 2010. Copyright (2010), with permission from Elsevier.).

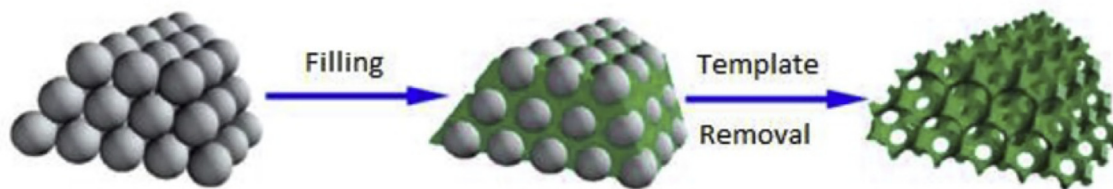


Fig. 19. Representation of synthesis by template method for TiO₂ inverse opal structure [95]. (Reprinted from Yu et al. 2018. Copyright (2018), with permission from Elsevier.).

6.5. Chemical vapor deposition (CVD)

Chemical Vapor Deposition (CVD) is one of the commonly used TiO_2 preparation techniques. One or more volatile materials, typically as mixed solid and gaseous precursors, are introduced in a reaction chamber under predetermined temperature and pressure. Depending on the anticipated reaction and relevant parameters it is possible to produce either TiO_2 powders or thin films [114]. The nucleation and growth mechanisms taking place in the nanoparticle formation can determine the morphology and phase and are often manipulatable when using CVD [115,116]. After the growth of the newly formed nucleation sites, various nanosized particles may be collected depending on reaction time and rate [117]. The formation mechanism of TiO_2 thin film is notably different than that used for nano-powder formation. First, the precursor(s) are evaporated and transferred to the reaction chamber by some carrier gas. Then, while in the reaction zone, the gaseous reactions occur; these reactants are transferred to, and adsorbed by, the heated substrate. Surface diffusion takes place and the nucleation and growth of the TiO_2 layer occur. The deposition rate of a film by CVD depends on several factors including the type of the carrier gas (this can be a reactant gas or inert gas such as H_2 , N_2 , and Ar), the type of the precursor material(s), the type and temperature of the substrate, the synthesis temperature, the deposition time, and the design of the reaction chamber [118-121].

Lee et al. [122] used TTIP as a precursor material to coat TiO_2 nanoparticles on glass beads using a CVD method. The precursor was evaporated and carried with carrier gasses (N_2 and Ar) at 900 °C to soda-lime glass beads. The effect of the deposition time on the photocatalytic performance was investigated and it was reported that a one-hour deposition had the best photocatalytic performance with respect to the decomposition of acetaldehyde.

Besides these above-mentioned methods, there are numerous comparable techniques including plasma-enhanced CVD (PECVD), physical vapor deposition (PVD), sputtering, pulsed laser deposition, and atomic layer deposition have been used to produce different TiO_2 nanostructures. When compared, all these techniques have both advantages and disadvantages between each other. Generally, there are several parameters with competing influences on the overall quality of the final TiO_2 nanostructure. All the techniques explained above and mentioned have a critical effect on the morphology and structure of TiO_2 , which determines the photoelectrocatalytic performance. Production techniques have a nontrivial impact on the detection limit and sensitivity of any TiO_2 PEC system. Therefore, more research should be conducted on the performance and photoelectrocatalytic COD determination of TiO_2 systems with respect to the production technique.

6.6. TiO_2 based nanocomposites

As seen in earlier sections, TiO_2 has been the most prevalent PEC material due to its numerous advantages. However, there are significant limitations and drawbacks; the main concern with TiO_2 is the wide indirect band gap energy. This limits the absorption of solar energy to 5% and permits a fast electron/hole recombination rate, lowering the overall quantum efficiency [123,124]. To minimize these drawbacks, researchers have been proposed various strategies, including metal/non-metal ion doping [125-127], heterojunction formation [128], morphological and structural modifications [129,130], sensitization [131], hydrogenation [132-134], etc. Recently, most of this attention has been directed to nanocomposite formation.

Introduction of another semiconductor material in TiO_2 systems is one of the common research directions taken to improve the photoelectrochemical and photocatalytic performance. The charge transfer between the different band gap structures and surface interactions coming from composite structures improve the photoelectrocatalytic performance of TiO_2 . Pang et al. [135] introduce a bismuth-based semiconductor in TiO_2 nanotubes arrays and they report an enhanced

photoelectrochemical COD detection with a sensitivity of 2.05 $\mu\text{A}\cdot\text{cm}^{-2}/(\text{mg}\cdot\text{L}^{-1})$ and with a detection range of 0.366 – 208.9 $\text{mg}\cdot\text{L}^{-1}$. Narrow bandgap semiconductors have also been combined with TiO_2 to enhance the photoelectrocatalytic activity under visible light illumination. To illustrate, Cu_2O (bandgap energy of Cu_2O is 1.9 eV) is loaded on TiO_2 nanotubes and this composite electrode show an enhanced photoelectrocatalytic activity relative to pure TiO_2 nanotubes under visible light illumination. A COD detection limit of 15 $\text{mg}\cdot\text{L}^{-1}$ with a linear range of 20–300 $\text{mg}\cdot\text{L}^{-1}$ is reported [136]. In addition to semiconductors, metal nanoparticles have also been incorporated into TiO_2 structures to form composite materials with enhanced COD detection. Si et al., load Au nanoparticles on 3D TiO_2 nanotube arrays, which demonstrated enhanced photoelectrocatalytic properties. They confirm known COD values of representative organic solutions with a detection limit of 0.18 $\text{mg}\cdot\text{L}^{-1}$ and linear detection range of 1.92 – 3360 $\text{mg}\cdot\text{L}^{-1}$ under UV illumination [85].

6.7. TiO_2 electrode preparation

TiO_2 nanostructures can be produced by several techniques, as explained. These TiO_2 nanostructures and the associated preparation methods are the most common choices for TiO_2 electrode fabrication. Typical TiO_2 electrode preparation is done by assembling a sensing electrode with either a conductive or nonconductive electrode substrate. Although conductive substrates are preferred for most applications, nonconductive substrates are often used in some gas sensors [137].

As the TiO_2 synthesis techniques are in solutions, deposition of the as prepared TiO_2 colloids onto a substrate surface plays a crucial role. Among the deposition methods, dip coating is the oldest and simplest technique. This technique involves a prepared substrate which is immersed into a TiO_2 containing solution at steady speed, then removed, the solvent is evaporated, depositing some thickness of TiO_2 . This technique is very useful to prepare uniform films. By controlling the dipping and removal speed, the overall thickness of the deposited film may be controlled [138]. Another very common deposition method to form TiO_2 thin films is spin coating [139]. With this method, the coating is spread by centrifugal forces. A fixed substrate is rotated at high speeds while some TiO_2 solution is deposited. The layer remains behind after evaporating the solvent. The thickness and uniformity of the film depend on the volume of deposited solution and the rotating speed. For PeCOD applications, the control of the film thickness and uniformity is the most important design factor. For large-scale and industrial applications, the production volume, cost, energy demand, complexity must additionally be considered. The reproducibility of the sensing slides fabrication by dip coating and spin coating techniques is not trivial and must be considered along with the variability related to solution preparation and deposition. Recently, inkjet printing techniques have been proposed for the fabrication of TiO_2 photoanodes for mass production of reproducible slides. By inkjet printing, as-synthesized TiO_2 colloids are immobilized on a desired substrate. The slides prepared by this technique have been used to determine COD of aqueous solutions, resulting in a linear range of 0–120 $\text{mg}\cdot\text{L}^{-1}$ with a detection limit of 1 $\text{mg}\cdot\text{L}^{-1}$ has been reported [140].

Many applications have functional requirements that cannot be met with pure TiO_2 nanomaterial electrodes. Consideration for heightened sensitivity, detection range, and response time must be incorporated into the electrode preparation method if the device must satisfy more stringent requirements for specific sensing applications. This is mostly applicable to bio- and gas-sensing applications, which has led to more severe limitations on their practical applications. Surface modification or surface functionalization are popular methods used to overcome these problems in TiO_2 electrodes. Generally, noble metals, polymers, and biomolecules are introduced to the TiO_2 films for specific, targeted

application purposes [141–143]. The greatest challenge to the integration and deposition of these materials is the prevalence of oxidation and corrosion after implementation, which decreases the specified performance [144].

TiO₂ nanomaterials are still a popular research topic, especially in sensing application fields. The continued focus revolves around developing better-performing sensors; this depends on the optimized processing of TiO₂ nanomaterials, electrode formation processes, and surface functionalization processes.

7. Conclusions

In this work, state-of-the-art PEC TiO₂ materials fabrication methods, testing, and characterization were discussed. Currently, a wide variety of manufacturing techniques have been developed. This makes the selection of a suitable manufacturing process and the corresponding implementation difficult for a particular industrial-scale sensing application.

Nevertheless, hydrothermal and electro-spinning techniques might be well-suited systems for simple or scalable production routes. More complicated techniques such as anodization, CVD, and inverse opal suffer from scalability or accessibility requirements. Consideration for heightened sensitivity, detection range, and response time must be incorporated into the electrode preparation method if the device must satisfy more stringent requirements for specific sensing applications. Many application-specific possibilities for material manipulation exist; typical, pragmatic implementations of TiO₂ involve an active layer fixed to a conductive substrate. The operation and implementation of sensors for COD are discussed with respect to our specific implemented system. The electrical, mechanical, theoretical, and practical aspects of the development of the system and their optimization are outlined. These factors are very application-dependent; however, catalytic systems generally rely on cycling between samples and calibration stages such that the reproducibility and minimization of variation are paramount. These catalytic systems rely on similar considerations for the adequate removal of contaminants, appropriate system geometries, and reproducible fabrication. Microfluidics are a common and challenging topic in the design and implementation of sensor systems, but the minimization of complexing aspects in photocatalytic systems enables a reliable and systematic implementation of PEC TiO₂ analyzers.

Declaration of Competing Interest

The authors declare that they have no known competing financial interests or personal relationships that could have appeared to influence the work reported in this paper.

Acknowledgments

B.B.A, A.G. and J.R.P contributed equally to this work. The authors' research is supported by MANTECH. B.B.A, A.G. and J.R.P. acknowledge the support of Canadian Mathematics of Information Technology and Complex Systems Agency (MITACS) [Grant No: IT17161, 2000–2024], NSERC Alliance [Grant No: ALLRP 554872 - 20] and Discovery [Grant No: GPIN-2020-06053] research programs.

References

- [1] AKIRA FUJISHIMA, KENICHI HONDA, Electrochemical Photolysis of Water at a Semiconductor Electrode, *Nature*. 238 (5358) (1972) 37–38.
- [2] World Health Organization, Drinking Water, (2019). <https://www.who.int/news-room/fact-sheets/detail/drinking-water>.
- [3] G. Divyapriya, S. Singh, C.A. Martínez-huitle, J. Scaria, A.V. Karim, P.V. Nidheesh, Treatment of real wastewater by photoelectrochemical methods : An overview, *Chemosphere*. 276 (2021), <https://doi.org/10.1016/j.chemosphere.2021.130188>.
- [4] M.J. Hammer, Water and wastewater technology, (1986).
- [5] D. Bahnemann, Photocatalytic water treatment : solar energy applications 77 (2004) 445–459, <https://doi.org/10.1016/j.solener.2004.03.031>.
- [6] Z. Sun, J.H. Kim, Y. Zhao, F. Bijarbooneh, V. Malgras, Y. Lee, Y.-M. Kang, S.X. Dou, Rational design of 3D dendritic TiO₂ nanostructures with favorable architectures, *J Am Chem Soc*. 133 (48) (2011) 19314–19317.
- [7] K. Nakata, A. Fujishima, TiO₂ photocatalysis: Design and applications, *Journal of Photochemistry and Photobiology C: Photochemistry Reviews*. 13 (3) (2012) 169–189, <https://doi.org/10.1016/j.jphotochemrev.2012.06.001>.
- [8] Z. Yu, H. Liu, M. Zhu, Y. Li, W. Li, Interfacial Charge Transport in 1D TiO₂ Based Photoelectrodes for Photoelectrochemical Water Splitting, *Small*. 17 (9) (2021) 1903378, <https://doi.org/10.1002/sml.v17.9.1002/sml.201903378>.
- [9] Q. Tay, X. Liu, Y. Tang, Z. Jiang, T.C. Sum, Z. Chen, Enhanced photocatalytic hydrogen production with synergistic two-phase anatase/brookite TiO₂ nanostructures, *The Journal of Physical Chemistry C*. 117 (29) (2013) 14973–14982.
- [10] A. Beltrán, L. Gracia, J. Andrés, Density Functional Theory Study of the Brookite Surfaces and Phase Transitions between Natural Titania Polymorphs, *The Journal of Physical Chemistry B*. 110 (46) (2006) 23417–23423.
- [11] J. Li, T. Ishigaki, X. Sun, Anatase, Brookite, and Rutile Nanocrystals via Redox Reactions under Mild Hydrothermal Conditions : Phase-Selective Synthesis and Physicochemical Properties, *The Journal of Physical Chemistry C*. 111 (2007) 4969–4976.
- [12] D.A.H. Hanaor, C.C. Sorrell, Review of the anatase to rutile phase transformation, *Journal of Materials Science*. 46 (4) (2011) 855–874, <https://doi.org/10.1007/s10853-010-5113-0>.
- [13] A. Sclafani, V. En, C. No, E.C. De Lyon, Comparison of the Photoelectronic and Photocatalytic Activities of Various Anatase and Rutile Forms of Titania in Pure Liquid Organic Phases and in Aqueous Solutions, *The Journal of Physical Chemistry*. 100 (1996) 13655–13661.
- [14] R. Thiruvenkatachari, S. Vigneswaran, I.S. Moon, A review on UV/TiO₂ photocatalytic oxidation process (Journal Review), *Korean Journal of Chemical Engineering*. 25 (1) (2008) 64–72.
- [15] K.L. Schulte, P.A. DeSario, K.A. Gray, Effect of crystal phase composition on the reductive and oxidative abilities of TiO₂ nanotubes under UV and visible light, *Applied Catalysis B: Environmental*. 97 (3-4) (2010) 354–360, <https://doi.org/10.1016/j.apcatb.2010.04.017>.
- [16] R. Yalavarthi, A. Naldoni, Š. Kment, L. Mascaretti, H. Kmentová, O. Tomanec, P. Schmuki, R. Zboržil, Radiative and non-radiative recombination pathways in mixed-phase TiO₂ nanotubes for PEC water-splitting, *Catalysts*. 9 (2) (2019) 204, <https://doi.org/10.3390/catal9020204>.
- [17] J. Bai, J. Li, Y. Liu, B. Zhou, W. Cai, A new glass substrate photoelectrocatalytic electrode for efficient visible-light hydrogen production : CdS sensitized TiO₂ nanotube arrays, *Applied Catalysis B: Environmental*. 95 (2010) 408–413, <https://doi.org/10.1016/j.apcatb.2010.01.020>.
- [18] S. Kawasaki, R. Takahashi, T. Yamamoto, M. Kobayashi, H. Kumigashira, J. Yoshinobu, F. Komori, A. Kudo, M. Lippmaa, Photoelectrochemical water splitting enhanced by self-assembled metal nanopillars embedded in an oxide semiconductor photoelectrode, *Nature, Communications*. 7 (1) (2016), <https://doi.org/10.1038/ncomms11818>.
- [19] Y.K. Kho, A. Iwase, W.Y. Teoh, L. Mädler, A. Kudo, R. Amal, Photocatalytic H₂ evolution over TiO₂ nanoparticles. The synergistic effect of anatase and rutile, *The Journal of Physical Chemistry C*. 114 (6) (2010) 2821–2829.
- [20] ASTM Standard D8084-17, Standard Test Method for Photoelectrochemical Oxygen Demand of Freshwater Sources for Drinking Water Treatment Plants and Treated Drinking Water, ASTM International, West Conshohocken, PA. (2017). <https://doi.org/10.1520/D8084-17>.
- [21] K. Aghasadeghi, M.J. Larocque, D.R. Latulippe, Towards the real-time monitoring of industrial wastewater treatment processes via photoelectrochemical oxygen demand measurements, *Environmental Science: Water Research & Technology*. 4 (3) (2018) 394–402, <https://doi.org/10.1039/C7EW00471K>.
- [22] C. Liu, H. Zhao, Z. Ma, T. An, C. Liu, L. Zhao, D. Yong, J. Jia, X. Li, S. Dong, Novel environmental analytical system based on combined biodegradation and photoelectrocatalytic detection principles for rapid determination of organic pollutants in wastewaters, *Environmental Science and Technology*. 48 (3) (2014) 1762–1768, <https://doi.org/10.1021/es4031358>.
- [23] Y. Han, J. Qiu, Y. Miao, J. Han, S. Zhang, H. Zhang, H. Zhao, Robust TiO₂/BDD heterojunction photoanodes for determination of chemical oxygen demand in wastewaters, *Analytical Methods*. 3 (2011) 2003–2009, <https://doi.org/10.1039/c1ay05193h>.
- [24] J.i. Li, G. Luo, LingJun He, J. Xu, J. Lyu, Analytical Approaches for Determining Chemical Oxygen Demand in Water Bodies: A Review, *Critical Reviews in Analytical Chemistry*. 48 (1) (2018) 47–65, <https://doi.org/10.1080/10408347.2017.1370670>.
- [25] A.K. Stoddart, G.A. Gagnon, Application of photoelectrochemical chemical oxygen demand to drinking water, *Journal-American Water Works Association*. 106 (9) (2014) E383–E390, <https://doi.org/10.5942/jawwa.2014.106.0106>.
- [26] B. Li, A.K. Stoddart, G.A. Gagnon, in: *Microbiological Sensors for the Drinking Water Industry*, International Water Association, 2018, pp. 197–209, https://doi.org/10.2166/9781780408699_0197.
- [27] Q. Zhang, L. Gao, J. Guo, Effects of calcination on the photocatalytic properties of nanosized TiO₂ powders prepared by TiCl₄ hydrolysis, *Applied Catalysis B: Environmental*. 26 (2000) 207–215.
- [28] M.A. Fox, M.T. Dulay, Heterogeneous Photocatalysis, *Chem Rev*. 93 (1) (1993) 341–357.
- [29] J. Zhang, P. Zhou, J. Liu, J. Yu, New understanding of the difference of photocatalytic activity among anatase, rutile and brookite TiO₂, *Physical*

- Chemistry Chemical Physics. 16 (38) (2014) 20382–20386, <https://doi.org/10.1039/C4CP02201G>.
- [30] C. Min, S. Won, K. Cho, M.R. Ho, Degradation of organic compounds in wastewater matrix by electrochemically generated reactive chlorine species: kinetics and selectivity, *Catalysis Today*. 313 (2018) 189–195, <https://doi.org/10.1016/j.cattod.2017.10.027>.
- [31] H. Zhao, D. Jiang, S. Zhang, K. Catterall, R. John, Development of a direct photoelectrochemical method for determination of chemical oxygen demand, *Anal Chem*. 76 (1) (2004) 155–160.
- [32] G. Cazaudehore, B. Schraauwers, C. Peyrelasse, C. Lagnet, F. Monlau, Determination of chemical oxygen demand of agricultural wastes by combining acid hydrolysis and commercial COD kit analysis, *Journal of Environmental Management*. 250 (2019) 109464, <https://doi.org/10.1016/j.jenvman.2019.109464>.
- [33] K. Lee, Y. Kim, H. Suzuki, K. Ikebukuro, K. Hashimoto, I. Karube, Disposable Chemical Oxygen Demand Sensor Using a Microfabricated Clark-Type Oxygen Electrode with a TiO₂ Suspension Solution, *Electroanalysis: An International Journal Devoted to Fundamental and Practical Aspects of, Electroanalysis*. 12 (2000) 1334–1338.
- [34] Y.-C. Kim, K.-H. Lee, S. Sasaki, K. Hashimoto, K. Ikebukuro, I. Karube, Photocatalytic sensor for chemical oxygen demand determination based on oxygen electrode, *Anal Chem*. 72 (14) (2000) 3379–3382.
- [35] J. Bai, B. Zhou, Titanium Dioxide Nanomaterials for Sensor Applications, *Chem Rev*. 114 (19) (2014) 1131–1176.
- [36] S. Garcia-Segura, E. Brillas, Applied photoelectrocatalysis on the degradation of organic pollutants in wastewaters, *Journal of Photochemistry & Photobiology, C: Photochemistry Reviews*. 31 (2017) 1–35, <https://doi.org/10.1016/j.jphotochemrev.2017.01.005>.
- [37] H. Rajput, E.E. Kwon, S.A. Younis, S. Weon, T.H. Jeon, W. Choi, K.-H. Kim, Photoelectrocatalysis as a high-efficiency platform for pulping wastewater treatment and energy production, *Chemical Engineering Journal*. 412 (2021) 128612, <https://doi.org/10.1016/j.cej.2021.128612>.
- [38] M.R. Hoffmann, S.T. Martin, W. Choi, D.W. Bahnemann, Environmental applications of semiconductor photocatalysis, *Chem Rev*. 95 (1) (1995) 69–96.
- [39] D. Jiang, H. Zhao, S. Zhang, R. John, Characterization of photoelectrocatalytic processes at nanoporous TiO₂ film electrodes: photocatalytic oxidation of glucose, *The Journal of Physical Chemistry B*. 107 (2003) 12774–12780.
- [40] S. Murgolo, C. De Ceglie, C. Di Iaconi, G. Mascolo, Novel TiO₂-based catalysts employed in photocatalysis and photoelectrocatalysis for effective degradation of pharmaceuticals (PhACs) in water: A short review., *Current Opinion in Green and Sustainable Chemistry*. 30 (2021) 100473, <https://doi.org/10.1016/j.cogsc.2021.100473>.
- [41] S. Zhang, H. Zhao, D. Jiang, R. John, Photoelectrochemical determination of chemical oxygen demand based on an exhaustive degradation model in a thin-layer cell, *Analytica Chimica Acta*. 514 (1) (2004) 89–97, <https://doi.org/10.1016/j.aca.2004.03.043>.
- [42] D. Jiang, H. Zhao, S. Zhang, R. John, Kinetic study of photocatalytic oxidation of adsorbed carboxylic acids at TiO₂ porous films by photoelectrolysis, *Journal of Catalysis*. 223 (2004) 212–220, <https://doi.org/10.1016/j.jcat.2004.01.030>.
- [43] S. Zhang, D. Jiang, H. Zhao, Development of chemical oxygen demand on-line monitoring system based on a photoelectrochemical degradation principle, *Environ Sci Technol*. 40 (7) (2006) 2363–2368.
- [44] R.W. Matthews, Purification of water with near-UV illuminated suspensions of titanium dioxide, *Water Res*. 24 (5) (1990) 653–660.
- [45] C.A. Martínez-Huitle, M. Panizza, Electrochemical oxidation of organic pollutants for wastewater treatment, *Current Opinion in Electrochemistry*. 11 (2018) 62–71, <https://doi.org/10.1016/j.coelec.2018.07.010>.
- [46] E. Zarei, R. Ojani, Fundamentals and some applications of photoelectrocatalysis and effective factors on its efficiency: a review, *Journal of Solid State Electrochemistry*. 21 (2) (2017) 305–336, <https://doi.org/10.1007/s10008-016-3385-2>.
- [47] C. Byrne, G. Subramanian, S.C. Pillai, Recent advances in photocatalysis for environmental applications., *Journal of Environmental, Chemical Engineering*. 6 (3) (2018) 3531–3555, <https://doi.org/10.1016/j.jece.2017.07.080>.
- [48] W. Xi, S.-U. Geissen, Separation of titanium dioxide from photocatalytically treated water by cross-flow microfiltration, *Water Research*. 35 (5) (2001) 1256–1262.
- [49] R. Molinari, M. Borgese, E. Drioli, L. Palmisano, M. Schiavello, Hybrid processes coupling photocatalysis and membranes for degradation of organic pollutants in water, *Catal Today*. 75 (1–4) (2002) 77–85.
- [50] A. Fujishima, K. Hashimoto, T. Iyoda, S. Fukayama, T. Yoshimoto, T. Saitoh, Window glass employing titanium dioxide photocatalyst, U.S. Patent No: 6,939,611, 2005.
- [51] J. Qiu, S. Zhang, H. Zhao, Recent applications of TiO₂ nanomaterials in chemical sensing in aqueous media., *Sensors & Actuators B: Chemical*. 160 (1) (2011) 875–890, <https://doi.org/10.1016/j.snb.2011.08.077>.
- [52] W. Choi, A. Termin, M.R. Hoffmann, Effects of metal-ion dopants on the photocatalytic reactivity of quantum-sized TiO₂ particles, *Angewandte Chemie International Edition in English*. 33 (10) (1994) 1091–1092.
- [53] E. Kusmirek, Semiconductor electrode materials applied in photoelectrocatalytic wastewater treatment—an overview, *Catalysts*. 10 (2020) 439.
- [54] J.P. Barham, B. König, Synthetic photoelectrochemistry, *Angewandte Chemie International Edition*. 59 (29) (2020) 11732–11747, <https://doi.org/10.1002/anie.v59.2910.1002/anie.201913767>.
- [55] D. Monllor-Satoca, M.I. Díez-García, T. Lana-Villarreal, R. Gómez, Photoelectrocatalytic production of solar fuels with semiconductor oxides: materials, activity and modeling, *Chemical Communications*. 56 (82) (2020) 12272–12289, <https://doi.org/10.1039/D0CC04387G>.
- [56] O.A. Arotiba, B.O. Orimolade, B.A. Koiki, Visible light-driven photoelectrocatalytic semiconductor heterojunction anodes for water treatment applications, *Current Opinion in Electrochemistry*. 22 (2020) 25–34, <https://doi.org/10.1016/j.coelec.2020.03.018>.
- [57] P. Alulema-Pullupaxi, P.J. Espinoza-Montero, C. Sigcha-Pallo, R. Vargas, L. Fernández, J.M. Peralta-Hernández, J.L. Paz, Fundamentals and applications of photoelectrocatalysis as an efficient process to remove pollutants from water: A review, *Chemosphere*. 281 (2021) 130821, <https://doi.org/10.1016/j.chemosphere.2021.130821>.
- [58] M.G. Peleyeju, O.A. Arotiba, Recent trend in visible-light photoelectrocatalytic systems for degradation of organic contaminants in water/wastewater, *Environmental Science: Water Research & Technology*. 4 (10) (2018) 1389–1411, <https://doi.org/10.1039/C8EW00276B>.
- [59] S. Zhang, L. Li, H. Zhao, A portable photoelectrochemical probe for rapid determination of chemical oxygen demand in wastewaters, *Environ Sci Technol*. 43 (20) (2009) 7810–7815.
- [60] L. Li, S. Zhang, H. Zhao, A low cost universal photoelectrochemical detector for organic compounds based on photoelectrocatalytic oxidation at a nanostructured TiO₂ photoanode, *Journal of Electroanalytical Chemistry*. 656 (1–2) (2011) 211–217, <https://doi.org/10.1016/j.jelechem.2010.11.017>.
- [61] Q. Zheng, B. Zhou, J. Bai, L. Li, Z. Jin, J. Zhang, J. Li, Y. Liu, W. Cai, X. Zhu, Self-organized TiO₂ nanotube array sensor for the determination of chemical oxygen demand, *Advanced Materials*. 20 (5) (2008) 1044–1049.
- [62] D.L. Jiang, R. John, G.-Q. Zhao, Novel photoelectrochemical oxygen demand assay, Australia Provisional Patent 2003901589, 2003.
- [63] Z.S. Hosseini, F. Haghparast, A.A. Masoudi, A. Mortezaali, Enhanced visible photocatalytic performance of un-doped TiO₂ nanoparticles thin films through modifying the substrate surface roughness, *Materials Chemistry and Physics*. 279 (2022) 125530, <https://doi.org/10.1016/j.matchemphys.2021.125530>.
- [64] B.N.J. Persson, O. Albohr, U. Tartaglino, A.I. Volokitin, E. Tosatti, On the nature of surface roughness with application to contact mechanics, sealing, rubber friction and adhesion, *Journal of Physics: Condensed Matter* 17 (1) (2005) R1–R62, <https://doi.org/10.1088/0953-8984/17/1/R01>.
- [65] J. Li, L. Zheng, L. Li, G. Shi, Y. Xian, L. Jin, Photoelectro-Synergistic Catalysis at Ti/TiO₂/PbO₂ Electrode and Its Application on Determination of Chemical Oxygen Demand., *Electroanalysis: An International Journal Devoted to Fundamental and Practical Aspects of, Electroanalysis*. 18 (22) (2006) 2251–2256, [https://doi.org/10.1002/\(ISSN\)1521-410910.1002/elan.v18:2210.1002/elan.200603644](https://doi.org/10.1002/(ISSN)1521-410910.1002/elan.v18:2210.1002/elan.200603644).
- [66] J. Li, L. Zheng, L. Li, G. Shi, Y. Xian, L. Jin, Ti/TiO₂ electrode preparation using laser anneal and its application to determination of chemical oxygen demand., *Electroanalysis: An International Journal Devoted to Fundamental and Practical Aspects of, Electroanalysis*. 18 (10) (2006) 1014–1018, [https://doi.org/10.1002/\(ISSN\)1521-410910.1002/elan.v18:1010.1002/elan.200503481](https://doi.org/10.1002/(ISSN)1521-410910.1002/elan.v18:1010.1002/elan.200503481).
- [67] Q. Mu, Y. Li, Q. Zhang, H. Wang, TiO₂ nanofibers fixed in a microfluidic device for rapid determination of chemical oxygen demand via photoelectrocatalysis, *Sensors and Actuators B: Chemical*. 155 (2) (2011) 804–809, <https://doi.org/10.1016/j.snb.2011.01.051>.
- [68] V. Zwilling, M. Aucouturier, E. Darque-Ceretti, Anodic oxidation of titanium and TA6V alloy in chromic media. An electrochemical approach, *Electrochimica Acta*. 45 (6) (1999) 921–929.
- [69] S. Ozkan, A. Mazare, P. Schmuki, Critical parameters and factors in the formation of spaced TiO₂ nanotubes by self-organizing anodization, *Electrochimica Acta*. 268 (2018) 435–447, <https://doi.org/10.1016/j.electacta.2018.02.120>.
- [70] Z. Ma, J. Gao, X. Wu, Y. Xie, H. Yuan, Y. Shi, Preparation of well-aligned TiO₂ nanotubes with high length-diameter aspect ratio by anodic oxidation method, *J Nanosci Nanotechnol*. 18 (8) (2018) 5810–5816, <https://doi.org/10.1166/jnn.2018.15397>.
- [71] S.P. Albu, A. Ghicov, J.M. Macak, P. Schmuki, 250 μm long ordered TiO₂ nanotubes with hexagonal self-ordering, *Physica Status Solidi (RRL)–Rapid Research Letters*. 1 (2) (2007) R65–R67, [https://doi.org/10.1002/\(ISSN\)1862-627010.1002/pssr.v1:210.1002/pssr.200600069](https://doi.org/10.1002/(ISSN)1862-627010.1002/pssr.v1:210.1002/pssr.200600069).
- [72] S. Ng, P. Kuberský, M. Krbal, J. Prikryl, V. Gärtnerová, D. Moravcová, H. Söpha, R. Zazpe, F.K. Yam, A. Jäger, L. Hromádka, L. Beneš, A. Hamáček, J.M. Macak, ZnO coated anodic 1D TiO₂ nanotube layers: efficient photo-electrochemical and gas sensing heterojunction, *Advanced Engineering Materials*. 20 (2) (2018) 1700589, <https://doi.org/10.1002/adem.201700589>.
- [73] O. Alev, S. Erdem, Z.Z. Oztürk, Improved gas sensing performance of p-copper oxide thin film / n-TiO₂ nanotubes heterostructure, *Journal of Alloys and Compounds*. 749 (2018) 221–228, <https://doi.org/10.1016/j.jallcom.2018.03.268>.
- [74] P.X. Zhao, Y. Tang, J. Mao, Y.X. Chen, H. Song, J.W. Wang, Y. Song, Y.Q. Liang, X. M. Zhang, One-dimensional MoS₂-decorated TiO₂ nanotube gas sensors for efficient alcohol sensing, *Journal of Alloys and Compounds*. 674 (2016) 252–258, <https://doi.org/10.1016/j.jallcom.2016.03.029>.
- [75] P. Roy, S. Berger, P. Schmuki, TiO₂ nanotubes: synthesis and applications, *Angewandte Chemie International Edition*. 50 (13) (2011) 2904–2939, <https://doi.org/10.1002/anie.201001374>.
- [76] M. Ge, C. Cao, J. Huang, S. Li, S. Zhang, S. Deng, Q. Li, K. Zhang, Y. Lai, Synthesis, modification, and photo / photoelectro catalytic degradation applications of TiO₂ nanotube arrays: a review, 5 (2016) 75–112, <https://doi.org/10.1515/ntrv-2015-0049>.
- [77] J.M. Macak, H. Tsuchiya, A. Ghicov, K. Yasuda, R. Hahn, S. Bauer, P. Schmuki, TiO₂ nanotubes: Self-organized electrochemical formation, properties and

- applications, *Current Opinion in Solid State and Materials Science*. 11 (1-2) (2007) 3–18, <https://doi.org/10.1016/j.cossms.2007.08.004>.
- [78] H. Sopha, L. Hromadko, K. Nechvilova, J.M. Macak, Effect of electrolyte age and potential changes on the morphology of TiO₂ nanotubes, *Journal of Electroanalytical Chemistry*. 759 (2015) 122–128, <https://doi.org/10.1016/j.jelechem.2015.11.002>.
- [79] O.K. Varghese, M. Paulose, C.A. Grimes, Long vertically aligned titania nanotubes on transparent conducting oxide for highly efficient solar cells, *Nat Nanotechnol*. 4 (9) (2009) 592–597, <https://doi.org/10.1038/nnano.2009.226>.
- [80] K. Yasuda, P. Schmuki, Control of morphology and composition of self-organized zirconium titanate nanotubes formed in (NH₄)₂SO₄/NH₄F electrolytes, *Electrochimica Acta*. 52 (12) (2007) 4053–4061, <https://doi.org/10.1016/j.jelechem.2006.11.023>.
- [81] P. Mazierski, M. Nischk, M. Gołkowska, W. Lisowski, M. Gazda, M. Jerzy, T. Klimczuk, A. Zaleska-medynska, Photocatalytic activity of nitrogen doped TiO₂ nanotubes prepared by anodic oxidation: The effect of applied voltage, anodization time and amount of nitrogen dopant, *Applied Catalysis B: Environmental*. 196 (2016) 77–88, <https://doi.org/10.1016/j.apcatb.2016.05.006>.
- [82] B. Munirathinam, H. Pydimukkala, N. Ramaswamy, L. Neelakantan, Influence of crystallite size and surface morphology on electrochemical properties of annealed TiO₂ nanotubes, *Applied Surface Science*. 355 (2015) 1245–1253, <https://doi.org/10.1016/j.apsusc.2015.08.017>.
- [83] Y. Feng, H.H.M. Rijnaarts, D. Yntema, Z. Gong, D.D. Dionysiou, Z. Cao, S. Miao, Y. Chen, Y. Ye, Y. Wang, Applications of anodized TiO₂ nanotube arrays on the removal of aqueous contaminants of emerging concern: A review, *Water Research*. 186 (2020), <https://doi.org/10.1016/j.watres.2020.116327> 116327.
- [84] Z. Zhang, X. Chang, A. Chen, Determination of chemical oxygen demand based on photoelectrocatalysis of nanoporous TiO₂ electrodes, *Sensors and Actuators B: Chemical*. 223 (2016) 664–670, <https://doi.org/10.1016/j.snb.2015.10.001>.
- [85] H. Si, X. Zhang, S. Lin, A simple flow injection sensing system for the real-time on-line determination of chemical oxygen demand based on 3D Au-NPs/TiO₂ nanotube arrays, *Frontiers in Materials*. 6 (2019) 1–7, <https://doi.org/10.3389/fmats.2019.00238>.
- [86] T. Kasuga, M. Hiramoto, A. Hoson, T. Sekino, K. Niihara, Formation of Titanium Oxide Nanotube, *Langmuir*. 14 (12) (1998) 3160–3163.
- [87] J. Yu, H. Yu, B. Cheng, C. Trapalis, Effects of calcination temperature on the microstructures and photocatalytic activity of titanate nanotubes, *Journal of Molecular Catalysis A: Chemical*. 249 (1-2) (2006) 135–142, <https://doi.org/10.1016/j.molcata.2006.01.003>.
- [88] J. Yu, H. Yu, Facile synthesis and characterization of novel nanocomposites of titanate nanotubes and rutile nanocrystals, *Mater Chem Phys*. 100 (2-3) (2006) 507–512, <https://doi.org/10.1016/j.matchemphys.2006.02.002>.
- [89] N. Liu, X. Chen, J. Zhang, J.W. Schwank, A review on TiO₂-based nanotubes synthesized via hydrothermal method: Formation mechanism, structure modification, and photocatalytic applications, *Catalysis Today*. 225 (2014) 34–51, <https://doi.org/10.1016/j.cattod.2013.10.090>.
- [90] M. Kobayashi, V. Petrykin, K. Tomita, M. Kakihana, Hydrothermal synthesis of brookite-type titanium dioxide with snowflake-like nanostructures using a water-soluble citratoperoxotitanate complex, *Journal of Crystal Growth*. 337 (1) (2011) 30–37, <https://doi.org/10.1016/j.jcrysgro.2011.09.046>.
- [91] G. Zhao, J. Xuan, Q. Gong, L. Wang, J. Ren, M. Sun, F. Jia, G. Yin, B.o. Liu, In situ growing double-layer TiO₂ nanorod arrays on new-type FTO electrodes for low-concentration NH₃ detection at room temperature, *ACS Applied Materials & Interfaces*. 12 (7) (2020) 8573–8582, <https://doi.org/10.1021/acsmi.9b20337> 10.1021/acsmi.9b20337.s001.
- [92] U. Alam, M. Fleisch, I. Kretschmer, D. Bahnemann, M. Muneer, One-step hydrothermal synthesis of Bi-TiO₂ nanotube / graphene composites: An efficient photocatalyst for spectral degradation of organic pollutants under visible light irradiation, *Applied Catalysis B: Environmental*. 218 (2017) 758–769, <https://doi.org/10.1016/j.apcatb.2017.06.016>.
- [93] J. Ben Naceur, F. Jrad, K. Souiwa, F. Ben Rhouma, R. Chtourou, Hydrothermal reaction time effect in wettability and photoelectrochemical properties of TiO₂ nanorods arrays films, *Optik (Stuttg)*. 239 (2021) 166794, <https://doi.org/10.1016/j.ijleo.2021.166794>.
- [94] J. Wang, G. Xu, X. Zhang, P. Zhai, J. Lv, D. Wang, Z. Zheng, Y. Wu, Photoelectrochemical performances of TiO₂ nanotube arrays hydrothermally treated in sulfide, *Applied Surface Science*. 363 (2016) 644–650, <https://doi.org/10.1016/j.apsusc.2015.12.038>.
- [95] J. Yu, J. Lei, L. Wang, J. Zhang, Y. Liu, TiO₂ inverse opal photonic crystals: Synthesis, modification, and applications-A review, *Journal of Alloys and Compounds*. 769 (2018) 740–757, <https://doi.org/10.1016/j.jallcom.2018.07.357>.
- [96] E. Halary-Wagner, F.R. Wagner, A. Brioude, J. Mugnier, P. Hoffmann, Light-Induced CVD of Titanium Dioxide Thin Films II: Thin Film Crystallinity, *Chemical Vapor Deposition*. 11 (2005) 29–37, <https://doi.org/10.1002/cvde.200306304>.
- [97] J.H. Moon, Y. Cho, S. Yang, Room Temperature Chemical Vapor Deposition for Fabrication of Titania Inverse Opals: Fabrication, Morphology Analysis and Optical Characterization, *Bull Korean Chem Soc*. 30 (2009) 2245–2248.
- [98] L. Liu, S.K. Karuturi, L.T. Su, A.I.Y. Tok, TiO₂ inverse-opal electrode fabricated by atomic layer deposition for dye-sensitized solar cell applications, *Energy & Environmental Science*. 4 (2011) 209–215, <https://doi.org/10.1039/c0ee00086h>.
- [99] J.S. King, E. Graugnard, C.J. Summers, TiO₂ inverse opals fabricated using low-temperature atomic layer deposition, *Advanced Materials*. 17 (8) (2005) 1010–1013, [https://doi.org/10.1002/\(ISSN\)1521-409510.1002/adma.v17:810.1002/adma.200400648](https://doi.org/10.1002/(ISSN)1521-409510.1002/adma.v17:810.1002/adma.200400648).
- [100] M. Wu, A. Zheng, F. Deng, B. Su, Significant photocatalytic activity enhancement of titania inverse opals by anionic impurities removal in dye molecule degradation, *Applied Catalysis B: Environmental*. 138 (2013) 219–228, <https://doi.org/10.1016/j.apcatb.2013.02.044>.
- [101] Jeremy W. Galusha, Chia-Kuang Tsung, Galen D. Stucky, Michael H. Bartl, Optimizing Sol - Gel Infiltration and Processing Methods for the Fabrication of High-Quality Planar Titania Inverse Opals, *Chemistry of Materials*. 20 (15) (2008) 4925–4930.
- [102] Dianyu Qi, Liujia Lu, Lingzhi Wang, Jinlong Zhang, Improved SERS sensitivity on plasmon-free TiO₂ photonic microarray by enhancing light-matter coupling, *J Am Chem Soc*. 136 (28) (2014) 9886–9889.
- [103] F. Sordello, V. Maurino, C. Minero, Photoelectrochemical study of TiO₂ inverse opals, *Journal of Materials Chemistry*. 21 (2011) 19144–19152, <https://doi.org/10.1039/c1jm12674a>.
- [104] V. Likodimos, Photonic crystal-assisted visible light activated TiO₂ photocatalysis, *Applied Catalysis B: Environmental*. 230 (2018) 269–303, <https://doi.org/10.1016/j.apcatb.2018.02.039>.
- [105] Tingting Wan, Seeram Ramakrishna, Yong Liu, Recent progress in electrospinning TiO₂ nanostructured photo-anode of dye-sensitized solar cells, *Journal of Applied Polymer Science*. 135 (1) (2018) 45649, <https://doi.org/10.1002/app.45649>.
- [106] N. Bhardwaj, S.C. Kundu, Electrospinning: A fascinating fiber fabrication technique, *Biotechnol Adv*. 28 (2010) 325–347, <https://doi.org/10.1016/j.biotechadv.2010.01.004>.
- [107] A. Sreekumar Nair, Yang Shengyuan, Zhu Peining, Seeram Ramakrishna, Rice grain-shaped TiO₂ mesostructures by electrospinning for dye-sensitized solar cells, *Chemical Communications*. 46 (39) (2010) 7421, <https://doi.org/10.1039/c0cc01490g>.
- [108] J. Yang, L. Pan, G. Zhu, X. Liu, H. Sun, Z. Sun, Electrospun TiO₂ microspheres as a scattering layer for CdS quantum dot-sensitized solar cells, *Journal of Electroanalytical Chemistry*. 677 (2012) 101–104, <https://doi.org/10.1016/j.jelechem.2012.05.018>.
- [109] B. Sun, Y.Z. Long, F. Yu, M.M. Li, H.D. Zhang, W.J. Li, T.X. Xu, Self-assembly of a three-dimensional fibrous polymer sponge by electrospinning, *Nanoscale*. 4 (2012) 2134–2137, <https://doi.org/10.1039/c2nr11782g>.
- [110] G. He, X. Wang, M. Xi, F. Zheng, Z. Zhu, H. Fong, Fabrication and evaluation of dye-sensitized solar cells with photoanodes based on electrospun TiO₂ nanotubes, *Materials Letters*. 106 (2013) 115–118, <https://doi.org/10.1016/j.matlet.2013.05.014>.
- [111] G. Ai, W.T. Sun, Y.L. Zhang, L.M. Peng, Nanoparticle and nanorod TiO₂ composite photoelectrodes with improved performance, *Chemical Communications*. 47 (2011) 6608–6610, <https://doi.org/10.1039/c1cc11092f>.
- [112] Joshua Zheyuan Soo, Kian Mun Lee, Bee Chin Ang, Boon Hoong Ong, Optimal electrospun TiO₂ nanofiber photocatalytic performance via synergistic morphology and particle crystallinity with anatase/rutile phase tuning, *Physica Status Solidi (a)* 216 (16) (2019) 1900066, <https://doi.org/10.1002/pssa.v216.1610.1002/pssa.201900066>.
- [113] Anitha Devadoss, Asako Kuragano, Chiaki Terashima, P. Sudhagar, Kazuya Nakata, Takeshi Kondo, Makoto Yuasa, Akira Fujishima, Single-step electrospun TiO₂-Au hybrid electrodes for high selectivity photoelectrocatalytic glutathione bioanalysis, *Journal of Materials Chemistry B*. 4 (2) (2016) 220–228, <https://doi.org/10.1039/C5TB01740H>.
- [114] Xingwang Zhang, Minghua Zhou, Lecheng Lei, Preparation of photocatalytic TiO₂ coatings of nanosized particles on activated carbon by AP-MOCVD, *Carbon* N Y. 43 (8) (2005) 1700–1708, <https://doi.org/10.1016/j.carbon.2005.02.013>.
- [115] Sakshum Khanna, Priyanka Marathe, Sagar Paneliya, Rakesh Chaudhari, Jay Vora, Fabrication of rutile-TiO₂ nanowire on shape memory alloy: a potential material for energy storage application, *Materials Today: Proceedings*. 50 (2022) 11–16, <https://doi.org/10.1016/j.matpr.2021.01.012>.
- [116] C. Liu, J. Camacho, H. Wang, Phase Equilibrium of TiO₂ Nanocrystals in Flame-Assisted Chemical Vapor Deposition, (2018) 180–186, <https://doi.org/10.1002/cphc.201700962>.
- [117] W. Li, S.I. Shah, C. Huang, O. Jung, C. Ni, Metallorganic chemical vapor deposition and characterization of TiO₂ nanoparticles, *Materials Science and Engineering: B*. 96 (2002) 247–253.
- [118] Chien-Sheng Kuo, Yao-Hsuan Tseng, Chia-Hung Huang, Yuan-Yao Li, Carbon-containing nano-titania prepared by chemical vapor deposition and its visible-light-responsive photocatalytic activity, *Journal of Molecular Catalysis A: Chemical*. 270 (1-2) (2007) 93–100, <https://doi.org/10.1016/j.molcata.2007.01.031>.
- [119] Xingwang Zhang, Minghua Zhou, Lecheng Lei, Preparation of an Ag-TiO₂ photocatalyst coated on activated carbon by MOCVD, *Materials Chemistry and Physics*. 91 (1) (2005) 73–79, <https://doi.org/10.1016/j.matchemphys.2004.10.058>.
- [120] Gianluca Li Puma, Awang Bono, Duduku Krishnaiah, Joseph G. Collin, Preparation of titanium dioxide photocatalyst loaded onto activated carbon support using chemical vapor deposition: a review paper, *Journal of Hazardous Materials*. 157 (2-3) (2008) 209–219, <https://doi.org/10.1016/j.jhazmat.2008.01.040>.
- [121] Naghme Aboualigadedari, Mohammad Rahmani, A review on the synthesis of the TiO₂-based photocatalyst for the environmental purification, *Journal of Composites and Compounds*. 2 (5) (2021) 25–42.
- [122] Heejin Lee, Min Young Song, Jongsoo Jung, Young-Kwon Park, The synthesis and coating process of TiO₂ nanoparticles using CVD process, *Powder*

- Technology. 214 (1) (2011) 64–68, <https://doi.org/10.1016/j.powtec.2011.07.036>.
- [123] Xiaobo Chen, Clemens Burda, The electronic origin of the visible-light absorption properties of C-, N- and S-doped TiO₂ nanomaterials, *J Am Chem Soc.* 130 (15) (2008) 5018–5019, <https://doi.org/10.1021/ja711023z>.
- [124] X. Chen, C. Li, M. Grätzel, R. Kostecki, S.S. Mao, *Nanomaterials for renewable energy production and storage*, *Chemical Society Reviews.* 41 (2012) 7909–7937, <https://doi.org/10.1039/c2cs35230c>.
- [125] M. Zhang, S. Yuan, Z. Wang, Y. Zhao, L. Shi, Photoelectrocatalytic properties of Cu₂₊-doped TiO₂ film under visible light, *Applied Catalysis B: Environmental.* 134 (2013) 185–192, <https://doi.org/10.1016/j.apcatb.2013.01.024>.
- [126] Bin Gao, Tao Wang, Xiaoli Fan, Hao Gong, Hu Guo, Wei Xia, Yaya Feng, Xianli Huang, Jianping He, Synthesis of yellow mesoporous Ni-doped TiO₂ with enhanced photoelectrochemical performance under visible light, *Inorganic Chemistry, Frontiers.* 4 (5) (2017) 898–906, <https://doi.org/10.1039/C6QI00609D>.
- [127] Yingzhi Chen, Aoxiang Li, Qun Li, Xinmei Hou, Lu-Ning Wang, Zheng-Hong Huang, Facile fabrication of three-dimensional interconnected nanoporous N-TiO₂ for efficient photoelectrochemical water splitting, *J Mater Sci Technol.* 34 (6) (2018) 955–960, <https://doi.org/10.1016/j.jmst.2017.07.010>.
- [128] Zhigang Wu, Jianling Zhao, Zekun Yin, Xiaoliu Wang, Ziqing Li, Xixin Wang, Highly sensitive photoelectrochemical detection of glucose based on BiOBr/TiO₂ nanotube array pn heterojunction nanocomposites, *Sensors and Actuators B: Chemical.* 312 (2020) 127978, <https://doi.org/10.1016/j.snb.2020.127978>.
- [129] Hwei Si, Nengqian Pan, Xidong Zhang, Jianjun Liao, M.N. Rumyantseva, A.M. Gaskov, Shiwei Lin, A real-time on-line photoelectrochemical sensor toward chemical oxygen demand determination based on field-effect transistor using an extended gate with 3D TiO₂ nanotube arrays, *Sensors & Actuators: B, Chemical.* 289 (2019) 106–113, <https://doi.org/10.1016/j.snb.2019.03.071>.
- [130] C. Feng, J.E. Soc, C. Feng, G. Xu, H. Liu, J. Lv, Z. Zheng, Y. Wu, A flow-injection photoelectrochemical sensor based on TiO₂ nanotube arrays for organic compound detection, *J Electrochem Soc.* 161 (2014) H57, <https://doi.org/10.1149/2.007403jes>.
- [131] Ruonan Wang, Meng Zu, Siyuan Yang, Shanqing Zhang, Wuyi Zhou, Ziyang Mai, Cunyu Ge, Yuehua Xu, Yueping Fang, Shengsen Zhang, Visible-light-driven photoelectrochemical determination of Cu²⁺ based on CdS sensitized hydrogenated TiO₂ nanorod arrays, *Sensors and Actuators B: Chemical.* 270 (2018) 270–276, <https://doi.org/10.1016/j.snb.2018.05.056>.
- [132] Meng Zu, Mengting Zheng, Shengsen Zhang, Chao Xing, Ming Zhou, Hu Liu, Xiaosong Zhou, Shanqing Zhang, Designing robust anatase-branch@hydrogenated-rutile-nanorod TiO₂ as accurate and sensitive photoelectrochemical sensors., *Sensors & Actuators: B, Chemical.* 321 (2020) 128504, <https://doi.org/10.1016/j.snb.2020.128504>.
- [133] Z. Liu, Y. Song, Q. Wang, Y. Jia, X. Tan, X. Du, S. Gao, Solvothermal fabrication and construction of highly photoelectrocatalytic TiO₂ NTs/Bi₂MoO₆ heterojunction based on titanium mesh, *Journal of Colloid And Interface Science.* 556 (2019) 92–101, <https://doi.org/10.1016/j.jcis.2019.08.038>.
- [134] Y. Wang, M. Zu, S. Li, T. Butburee, L. Wang, F. Peng, S. Zhang, Dual modification of TiO₂ nanorods for selective photoelectrochemical detection of organic compounds., *Sensors & Actuators: B, Chemical.* 250 (2017) 307–314, <https://doi.org/10.1016/j.snb.2017.04.113>.
- [135] Yajun Pang, Guangqing Xu, Qiang Feng, Jiaqin Liu, Jun Lv, Yong Zhang, Yucheng Wu, Synthesis of α-Bi₂Mo₃O₁₂/TiO₂ nanotube arrays for photoelectrochemical COD detection application, *Langmuir.* 33 (36) (2017) 8933–8942, <https://doi.org/10.1021/acs.langmuir.7b01826>.
- [136] C. Wang, J. Wu, P. Wang, Y. Ao, J. Hou, J. Qian, Photoelectrocatalytic determination of chemical oxygen demand under visible light using Cu₂O-loaded TiO₂ nanotube arrays electrode, *Sensors and Actuators B: Chemical.* 181 (2013) 1–8, <https://doi.org/10.1016/j.snb.2013.02.011>.
- [137] H. Kim, M. Hong, H. Won, S. Yoon, H. Park, CO gas sensing properties of direct-patternable TiO₂ thin films containing multi-wall carbon nanotubes, *Thin Solid Films.* 529 (2013) 89–93, <https://doi.org/10.1016/j.tsf.2012.07.062>.
- [138] M. Shakeel, A.K. Pandey, N. Abd, Advancements in the development of TiO₂ photoanodes and its fabrication methods for dye sensitized solar cell (DSSC) applications, A review, *Renewable and Sustainable Energy Reviews.* 77 (2017) 89–108, <https://doi.org/10.1016/j.rser.2017.03.129>.
- [139] M. Arman, L. Zakir, H. Zikriya, K. Muhammad, A. Akram, A. Shuja, Effects of Ag doping on compact TiO₂ thin films synthesized via one – step sol – gel route and deposited by spin coating technique, *Journal of Materials Science: Materials in Electronics.* 31 (2020) 7172–7181, <https://doi.org/10.1007/s10854-020-03288-9>.
- [140] Min Yang, Lihong Li, Shanqing Zhang, Guiying Li, Huijun Zhao, Preparation, characterisation and sensing application of inkjet-printed nanostructured TiO₂ photoanode, *Sensors and Actuators B: Chemical.* 147 (2) (2010) 622–628, <https://doi.org/10.1016/j.snb.2010.03.048>.
- [141] Shuilin Wu, Zhengyang Weng, Xiangmei Liu, K.W. K. Yeung, Paul. K. Chu, Functionalized TiO₂ based nanomaterials for biomedical applications, *Adv Funct Mater.* 24 (35) (2014) 5464–5481, <https://doi.org/10.1002/adfm.v24.3510.1002/adfm.201400706>.
- [142] Jing Li, Hua Chun Zeng, Size tuning, functionalization, and reactivation of Au in TiO₂ nanoreactors, *Angewandte Chemie International Edition.* 44 (28) (2005) 4342–4345, [https://doi.org/10.1002/\(ISSN\)1521-377310.1002/anie.v44:2810.1002/anie.200500394](https://doi.org/10.1002/(ISSN)1521-377310.1002/anie.v44:2810.1002/anie.200500394).
- [143] Oleg Lupan, Vasile Postica, Nicolai Ababii, Tim Reimer, Sindu Shree, Mathias Hoppe, Oleksandr Polonskyi, Victor Sontea, Steffen Chemnitz, Franz Faupel, Rainer Adelung, Ultra-thin TiO₂ films by atomic layer deposition and surface functionalization with Au nanodots for sensing applications, *Materials Science in Semiconductor Processing.* 87 (2018) 44–53, <https://doi.org/10.1016/j.mssp.2018.06.031>.
- [144] Jianwei Su, Yunxia Zhang, Sichao Xu, Shuan Wang, Hualin Ding, Shusheng Pan, Guozhong Wang, Guanghai Li, Huijun Zhao, Highly efficient and recyclable triple-shelled Ag@ Fe₃O₄@SiO₂@TiO₂ photocatalysts for degradation of organic pollutants and reduction of hexavalent chromium ions, *Nanoscale.* 6 (10) (2014) 5181, <https://doi.org/10.1039/c4nr00534a>.